Abstract

Annamarie Lembares STUDY OF SOFT TISSUE INTERACTION WITH OPTICAL RADIATION. (Under the direction of Dr. Xin-Hua Hu) Department of Physics, April 1997.

The purpose of this thesis is to study the interaction between optical radiation and soft tissues. This is an initial part of a long-term research project to develop a clear understanding of the fundamental mechanisms underlying tissue ablation using short laser pulses. The thesis study is separated into two parts. In the first part, we investigate the absorbance spectra of corneas in a wide spectral region from 2600 to 190nm using a dual-beam spectrophotometer. For the first time, we measure the far ultraviolet absorption spectra of porcine and human corneas from 230 to 190nm. The experimental results show three distinct segments in corneal absorption in the far ultraviolet region. The linear absorption coefficients are determined from the absorbance spectra at specific wavelengths. Furthermore, a "window of ablation" in the far ultraviolet region between 220 and 190nm is determined. We conduct a statistical analysis to correlate the far ultraviolet absorption between the porcine and human corneas and investigate the effect of freezing on the far ultraviolet, visible and infrared absorption. The second part of the thesis study concentrates on skin tissue ablation using nanosecond pulses. Various tissue-processing techniques are tested for the quantitative measurement of ablation parameters. A set of procedures are identified and refined that can well control tissue conditions for histology examination. This provides a solid foundation for a quantitative investigation of surface ablation of skin tissue samples.

Study of Soft Tissue Interaction with Optical Radiation

A Thesis

Presented to

the Faculty of the Department of Physics

East Carolina University

In Partial Fulfillment

of the Requirements for the Degree

Master of Physics in Physics

by

Annamarie Lembares

April 1997

Study of Soft Tissue Interaction with Optical Radiation

by

Annamarie Lembares

APPROVED BY:

DIRECTOR OF THESIS_____
XIN-HUA HU, Ph.D.

CHAIR OF THE DEPARTMENT OF PHYSICS AND COMMITTEE MEMBER

_____
MUMTAZ A. DINNO, Ph.D.

COMMITTEE MEMBER_____
GERHARD W. KALMUS, Ph.D.

COMMITTEE MEMBER_____
GEORGE A. BISSINGER, Ph.D.

DEAN OF THE GRADUATE SCHOOL_____
THOMAS L. FELDBUSH, Ph.D.

Table of Contents

List of Tables

List of Figures

List of Symbols and Abbreviations

α.. linear absorption coefficient

A.. absorbance measurement from spectrophotometer

A/D... analog/digital

ArF.. argon fluorine excimer laser

d.. cornea section thickness

ETOH.. ethanol alcohol

GAH.. glutaraldehyde

I.. intensity of light on the sample

I_o.. intensity of transmitted light through the sample

IR... infrared

LIF... laser induced fluorescence

M... molar

mid-IR... mid-infrared

NIR.. near-infrared

ns.. nanosecond

R... Fresnel reflectivity of the glass-cornea interfaces

OCT... freezing preservation medium

σ.. standard deviation

T.. transmittance

UV... ultraviolet

VIS………………………………. visible

VIS-IR…………………………... visible and infrared

Chapter 1: Background

1.1 Introduction

Albert Einstein's model of radiation-matter interaction gave life to the concepts and principles necessary to create a functional laser. However, almost 38 years passed before an ammonia gas MASER, the first device to utilize these concepts, was developed by C.H. Townes with assistance from J.P. Gordon and H. Zeigerin in the U.S., and followed closely by N.G. Basov and A.M. Prokhorov in the Soviet Union. From 1956 to 1958, N. Bloembergen and C.H. Townes suggested infrared and optical lasers. The first functional laser system was developed by T.H. Maiman in 1960 with a ruby crystal.[1] Since then laser technology has been dramatically improved and immediately adopted for medical uses.

The past three decades has refined "laser" technology and enabled the medical use of lasers to prosper. The pioneers of laser surgery used the intense heat generated by the beam of light in the forms of continuous-wave or long pulses for its ablative and coagulate effects which can be very selective and well controlled.[2] In addition to heating the tissue, photons from laser pulses can induce chemical reactions, break atomic and molecular bonds, and produce shock waves and various acoustic transients. These forms of interactions could lead to ablation, the removal of tissue, when the wavelength, duration of laser pulse, and pulse energy are matched with the specific physical and chemical properties of the target tissues.[3,4] The target tissue can be characterized by the following properties: optical (absorption and scattering); thermal (heat capacity and

diffusivity); mechanical (viscoelasticity and tensile strength); chemical (water and other chromophores); anatomy (arrangement of organelles, cells and tissues); and physiology (metabolic states and functions).[3] For the conversion of the laser light energy into other forms of energy in a specified target tissue, the absorption property is one of the most important tissue parameters. The absorption of laser radiation in the targeted tissue is caused by chromophores. A chromophore is a molecule, or a portion of a molecule, that absorbs light of a particular wavelength. The absorption of the photon's energy by tissue chromophores relates closely to the ablation process of the tissue.[5-8]

In the medical field, nanosecond laser pulses are of great interest for precision surgery. The pulses can be generated by Q-switched lasers of simple structures in comparison with other short pulsed lasers. A Q-switched laser contains an intracavity shutter that remains closed and thus prevents light amplification inside the cavity until a large population inversion is attained inside the gain medium of the laser. At the appropriate time, the intracavity shutter is opened to allow the occurrence of light amplification. Oscillation and amplification follow quickly with emission of a short high-energy pulse of duration ranging from 1 to 100ns. The "Q" refers to the quality factor of the laser cavity defined as the quotient of the energy in the cavity and the energy lost per cycle of oscillation. Rapid extraction of high power is accomplished as the intracavity shutter switches the "Q" of the cavity.

Ablation-based laser surgery using nanosecond laser pulses is being actively studied due to the potential of high precision and little collateral tissue damage. However, the fundamental mechanisms of tissue ablation by nanosecond laser pulses

have not been clearly understood. Three major models have been proposed to explain the soft tissue ablation by nanosecond laser pulses in the spectral region from far ultraviolet (UV) to near-infrared (NIR): the selective photothermolysis model, the photochemical model, and the plasma mediated ablation model.

The selective photothermolysis model assumes a thermal ablation mechanism in soft tissue ablation with visible and NIR laser pulses.[5] Due to the target tissue's characteristic absorption properties, the target tissue can be ablated with limited damage to the collateral tissue if the target has a greater optical absorption than the collateral tissue at the wavelength of the laser pulse and if the laser pulse has a duration shorter than the time for heat to diffuse into collateral tissue.[5] In general, thermal ablation models consider only the conversion of optical energy from the laser light into thermal energy in tissue.[6] When the laser irradiance (the peak power divided by the illuminated area) approaches the ablation threshold, rapid heating leads to the vaporization of water in the soft tissue. In turn, there is a steep increase in the internal pressure of the exposed tissue. Once the pressure overcomes the tensile strength of the tissue, ablation occurs.

The photochemical model has been the conventional model for corneal ablation by far UV nanosecond pulses. It assumes that high-energy photons (~ 6 eV) break down macromolecules in the cornea. When the laser irradiance exceeds the ablation threshold, the fragmentation process becomes the major channel of molecular relaxation. Tissue ablation is accomplished by the expulsion of molecular fragments from the tissue with the excess energy after the breakage of the chemical bonds.[9] Both of the above ablation models assume that ionization does not occur above the ablation threshold and the

ablation rate is primarily determined by pigment or chromophore absorption in the target tissue.[5,9]

Another model that has been used to describe the corneal ablation with nanosecond laser pulses at visible and NIR wavelengths is the plasma mediated ablation model.[7,10] A very short laser pulse produces an electromagnetic field that is high enough to breakdown the tissue through the creation of a highly energized gas of ions and electrons, also known as a plasma. When the laser irradiance reaches the ablation threshold, enough free electrons are generated to initialize an avalanche to form a plasma. The electrons in a plasma can effectively absorb photon energy from the laser pulse which results in a steep increase of temperature to 10^4 K or higher. The resultant high pressure from the plasma causes tissue ablation. When it cools down, shock wave and acoustic transients are generated to dissipate the energy in all directions which cause collateral tissue damage proportional to the energy deposited in tissue.[7,10,11] It has been widely accepted that the ablation of the cornea in the spectral region of visible and NIR occurs only when a plasma is formed because the tissue absorption in this spectral region is negligible.[7,10]

These different models have led to different designs of nanosecond laser systems for surgery, but each with the same goal: to efficiently ablate the target tissue with minimal damage to collateral tissue. However, the different ablation models for nanosecond laser pulses utilize assumptions that are not compatible to each other. Furthermore, the selective photothermolysis and photochemical models are not consistent with some important experimental results and the plasma model has not answered certain

fundamental questions such as the relation between tissue absorption and the formation of a plasma. This strongly indicates the need for a clear understanding of the fundamental mechanisms underlying soft tissue ablation using nanosecond laser pulses. For example, the investigation of corneal ablation curves by nanosecond laser pulses at 193nm and picosecond pulses at 211nm indicates that the measured ablation rates are far from the values predicted by the photochemical model.[8,12] Furthermore, several research groups including this lab have observed laser induced fluorescence (LIF) in corneal ablation by nanosecond pulses at 193nm and skin ablation by visible and NIR pulses.[13-15] At high laser irradiance, the LIF spectrum resembles closely to the blackbody radiation measured from water due to the optical breakdown induced by visible nanosecond pulses. These results suggest that temperature in the ablation area can reach up to 10^4 K for which the photochemical and the selective photothermolysis models do not provide a convincing explanation. Based on these considerations, it is very possible that plasma is formed in the corneal ablation by far UV nanosecond laser pulses and in skin ablation by visible and NIR nanosecond pulses. However, the source of the initial free electrons for the plasma formation in soft tissue ablated by nanosecond pulses has not been identified. These fundamental questions can only be answered through a detailed study of the interaction between optical radiation and soft tissue and the ablation process by nanosecond laser pulses in a wide spectral region from far UV to VIS-IR. This is undertaken by the studies presented in this thesis as an initial part of a long-term research project.

The study presented here is divided into two major parts. In part one we measure the absorption spectra of corneas in a wide spectral region from 2600 to 190nm, using a

dual-beam spectrophotometer, and study the far UV absorption of corneas from 350 to

190nm. The absorbance curves of the corneas are also compared with that of distilled

water to develop a better understanding of the role of water in the absorption for each

spectral region. The linear absorption coefficients are calculated from the absorbance

measurement at 220, 215, 210, and 193nm. Statistical analysis is performed to correlate

the far ultraviolet absorption spectra between the porcine and human corneas at the above

wavelengths. The effect of tissue conditions on the far ultraviolet absorption due to

procedural methods is also investigated. This enables the direct correlation of corneal

ablation with nanosecond laser pulses from solid state lasers near 210nm to the results of

ArF excimer lasers at 193nm since the ablation process strongly depends on the far UV

absorption. The second part of the thesis study deals with the investigation and

identification of optimal processing procedures for ablated soft tissue and skin ablation

using nanosecond laser pulses. It is mainly devoted to analysis of ablated skin tissue to

quantitatively measure the ablation depth as a function of laser pulse energy and spot size

of nanosecond laser pulses at 1064nm using a Q-switched Nd:YAG laser system. For this

purpose, histology techniques for studying surface ablation of the soft tissue samples are

performed.

1.2 Part One: Cornea Absorption Study

Nanosecond ultraviolet laser pulses from the excimer (ArF) laser are used

clinically to correct refractive errors of the eye through surface ablation of the cornea. It

is well known that the cornea strongly absorbs far UV radiation at 193nm[16] which makes

the ArF laser systems the current choice for precise ablation of the cornea. Hence, a significant amount of data has been collected on the corneal ablation at 193nm for the excimer laser systems.[16-18] But excimer lasers pose safety issues in clinics because of the toxic gases used as the gain medium. These gas laser systems are also undesirable for their low energy efficiency, large size and high maintenance cost. Solid state laser systems, together with a nonlinear harmonic generator, are being investigated as a possible replacement to the ArF laser systems for treating refractive errors of the eye through corneal ablation. The solid state laser systems can provide short UV pulses through harmonic generation at wavelengths near 210nm.[8,19] These laser systems use solid state materials as the gain medium and thus avoid the shortcomings of the gas systems mentioned above. However, the measurement of the corneal absorption between 190 to 230nm has not been reported.[20] Thus, it is difficult to directly correlate corneal ablation with solid state laser pulses near 210nm to the results of the ArF lasers at 193nm since the ablation process strongly depends on the far UV absorption.

An earlier investigation of corneal ablation with picosecond laser pulses at 211 and 263nm suggests that the corneal absorption in the far UV region may be divided into three segments based on the analysis of damage zones in collateral tissue.[8] It is concluded that the corneal absorption is relatively weak from 266 to 248nm, increases steeply from 248 to 213nm, and remains strong from 213 to 193nm. A plasma model assisted by chromophore absorption is proposed to explain the corneal ablation by both picosecond and nanosecond UV laser pulses.[8] Using this model it is suggested that the threshold of laser ablation of the cornea depends on both linear absorption coefficient of

the cornea and the duration of the laser pulses. By measuring the linear absorption coefficient in the far UV spectral region, the above hypothesis can be indirectly tested.

Following the above investigation, we set out to extend the measurement of the corneal absorption to the mid-IR region. It is well known that the cornea is transparent in the visible and mid-IR regions.[21] However, corneal absorption in the mid-IR region (up to 3000nm) has not been directly measured. The VIS-IR absorption spectrum of cornea is expected to mirror the absorption spectrum of water that accounts for more than 70% of wet weight of cornea. The objective of this part of the research is to provide a detailed absorption spectra of both the cornea and water in the IR region from 3000 to 1000nm. These results are very important for the clear understanding of the corneal ablation near 2000 and 3000nm. Due to the limitation of our spectrophotometer, we only complete the absorption spectra from 2600 to 600nm. In measurements to be performed in near future, the spectrum will be extended to 3000nm for both the cornea and water. With the absorbance measurement in this spectral region, we also investigate the effects of the freezing on corneal absorbance.

1.3 Part Two: Skin Ablation Study

The ablation-based laser surgery in dermatology with nanosecond laser pulses has gained increasing acceptance in the last decade.[22] As discussed earlier, we are interested in the study of the fundamental mechanism underlying the skin tissue ablation by nanosecond laser pulses. For this purpose we want to determine an appropriate animal model for the study of skin tissue ablation and identify optimal procedures for tissue

processing to obtain quantitative measurement of ablation parameters. Human skin has many peculiar properties that make finding an animal model difficult. Many laboratory animals demonstrate distinct morphologic differences from human skin: the epidermis is thinner, lacks basal cell heterogeneity and has a relatively flat dermal-epidermal junction.[23] It is postulated that one of the reasons for the epidermal differences is the protective fur coat.[24] Lavker *et al*. report that the Yucatan hairless micropig shows important similarities in morphology, cellular compositions, and immunoreactivity to the human plantar and palmar skin and responds similarly pharmacologically.[25] The features that are similar to human skin, and important in the ablation of the tissue, are skin pigmentation, keratin filaments, and melanocytes. Therefore, the hairless micropig offers several advantages over other laboratory animals for the evaluation of cutaneous interactions, such as with laser pulses. Bartell *et al.* also show that the skin of human and younger porcine have comparable hair density and an epidermal layer of similar thickness.[26] They also observe that porcine has a tighter collagen-reticulin packing than human skin.

The purpose of this part of the thesis study is to develop a histology technique to reliably measure the ablation depth per pulse as a function of laser pulse energy and spot size of nanosecond laser pulses at 1064nm using a Q-switched Nd:YAG laser system. Fresh skin from young porcine is used to better understand the fundamental mechanisms involved for skin tissue ablation. Different tissue processing techniques are studied to identify an optimal approach for histology examination that will produce minimal artifacts interfering with the measurement of the ablation cuts.

Chapter 2: Experimental Methods

2.1 Part One

2.1.1 Cornea Samples

Porcine and human corneas are used for the absorbance measurements. Institutional guidelines regarding the use of tissue and organs are followed. Fresh porcine eye globes are obtained from Robersonville Meats, Inc. (Robersonville, NC) and the School of Medicine, East Carolina University. The protocol for the use of animal tissues is approved by the University Animal Care and Use Committee. All procedures involving animals are performed in compliance with the ARVO Statement for the Use of Animals in Ophthalmic and Vision Research. A total of 23 cornea sections from 18 porcine corneas and 6 whole porcine corneas are used for the absorbance measurements where some of the measurements come from the same cornea. All eye globes are removed from the animals immediately after death and stored on ice until the corneas are excised from the globes. Absorbance measurements of the porcine cornea sections are performed within 12 hours postmortem except those samples used for studying the effect of freezing. Human corneas are provided by the North Carolina Eye and Human Tissue Bank, Inc. (Winston-Salem, NC). A total of 11 cornea sections from 5 fresh human corneas and 1 preserved cornea are used for the absorbance measurements where some of the measurements come from the same cornea. The absorbance measurements of the

fresh human cornea sections are performed within 33 hours postmortem and the preserved human cornea section at 1 week postmortem.

2.1.2 Excising the Cornea from the Eye Globe

The eye globes are stored on ice until the corneas are excised from the globe. To excise the cornea from the eye globe, a small hole is made through the eye globe near the conjunctiva. From this small hole the cornea is excised by cutting along the conjunctiva. The cornea is then removed, rinsed and stored in 0.9% saline solution and kept on ice until sectioning.

2.1.3 Sectioning of the Corneas

For UV absorbance measurements, the section thickness needs to be in the neighborhood of 20μm to keep the absorbance within the scale of the spectrophotometer because the cornea strongly absorbs in this spectral region. To obtain a thin contiguous cornea section of uniform thickness, a microtome-cryostat (Model 4551, Ames Company) is used to section the frozen cornea at -18 °C (see Appendix A). The excised cornea is frozen in the cryostat for 15 minutes or longer before sectioning. The superficial layers of the cornea, including the epithelium and the Bowman's layer, are removed until a uniform section from the corneal stroma is obtained. The cornea section is then transferred to a sample holder.

For VIS-IR absorbance measurements, the whole cornea with a thickness near 800μm is used because the cornea does not absorb as strongly as the far UV wavelengths.

Therefore, the excised cornea is transferred to the sample holder without the sectioning process.

2.1.4 Sample Holder

2.1.4.1 Cornea Absorbance Measurement

In the UV absorbance measurements, two rectangular optical windows made of UV grade fused silica glass (Type 7940, Corning Inc.) are used as a sample holder to keep the thin cornea section intact and total absorbance low for the UV absorbance measurements. The sample holder has a total thickness of ~12mm and a very low thermal expansion coefficient that helps to protect the cornea section in the course of thawing and transferring to the spectrophotometer. The absorbance of the sample holder increases slowly as the wavelength decreases in the far UV region (see Figure 1), which is measured to be less than 0.01 at 260nm and 0.011 at 190nm after the surface reflection contribution is deducted.

Before the cornea section is transferred to the sample holder, the optical windows are cleaned thoroughly with acetone. The cornea section is sandwiched between the two optical windows and clamped by a holder as shown in Figures 2 and 3. This helps to prevent dehydration of the section during the absorbance measurement and to remove any trapped air bubbles in the section. Two blackened metal plates with an aperture of 4mm in diameter for each are used at the front and back surfaces of the sample holder to collimate the incident and transmitted light beams, as shown in Fig.4.

For VIS-IR absorbance measurements the whole cornea is sandwiched between the same two optical windows used for the UV absorbance measurements to prevent the cornea from dehydrating during the measurement. The absorbance of the sample holder in the VIS-IR region is shown in Figure 5. The sample aperture plates are also used at the front and back surfaces of the sample holder to collimate the incident and transmitted beams.

2.1.4.2 Distilled Water Absorbance Measurement

For both the UV and VIS-IR absorbance measurements of distilled water, quartz cuvettes (Type 9, Starna Cells, Inc.) are used with a 10mm path length. The cuvettes are cleaned thoroughly with acetone. The sample cuvette is rinsed several times and filled with distilled water before the absorbance measurement. The sample and reference aperture plates are used for the VIS-IR absorbance measurement but are removed for the UV measurement due to the small absorbance signal.

2.1.5 Absorbance Measurement

The absorbance measurements of the cornea sections, whole cornea, and distilled water in the far UV region from 350 to 190nm and in the VIS-IR region from 2600 to 600nm are carried out a room temperature with a dual-beam UV-VIS-IR spectrophotometer (Model 17D, Varian Associates). Figure 6 shows the schematic of the spectrophotometer. The absorbance reading (A) obtained from the spectrophotometer is

the logarithmic ratio of the incident light on the sample I_o (measured from the reference

beam in the reference chamber) and the transmitted light through the section I (from the

sample beam through the sample chamber),

$$A = \log_{10}(\frac{I_o}{I}). \qquad\qquad (1)$$

The spectrophotometer can be used to measure absorbance from 0.0 to 3.0 in 5 scales

between 2600 and 190nm in wavelength. The UV wavelength reading is calibrated

using a standard UV mercury lamp and the absorbance reading with a dye solution of

known absorbance (see Appendix B). Both are found to be within the manufacturer's

specifications. The VIS-IR wavelength reading has yet to be calibrated. The output

signal from the spectrophotometer is digitized and averaged by a personal computer with

an A/D board.

The sample holder with the cornea section or whole cornea is placed in the sample

chamber while the reference chamber only contains the two identical apertures of 4mm in

diameter. Starting at 350nm, for the UV absorbance measurements, or 2600nm, for the

VIS-IR absorbance measurements, the spectrophotometer measures the total absorbance

of the sample holder and the corneal sample. When the absorbance reading reaches the

about one third of the full scale for a decreasing reading or about two thirds of the full

scale for an increasing reading, the scale is changed accordingly to accommodate the level

of absorption with the best sensitivity. The different segments of the same absorbance

measurement are overlapped to ensure accurate reading over the whole spectrum (see

Appendix C). The process is repeated until the minimum wavelength of 190nm is

reached for the UV absorbance measurements and 600nm for the VIS-IR absorbance

measurements (see Appendix D). Then the *difference* between the absorbance reading

and the absorbance of the sample holder without the corneal sample is plotted against the

wavelength (see Appendix C and D).

For the distilled water absorbance measurements, an empty cuvette is placed in

the reference chamber and a cuvette filled with distilled water in the sample chamber.

For the VIS-IR absorbance measurements, both chambers contain the two identical

apertures of 4mm in diameter. Because of the small signal for the UV absorbance reading

of the distilled water, the two identical apertures are removed from both chambers. The

UV and VIS-IR absorbance spectra are measured using the same procedure as the cornea.

However, the absorbance measurement obtained by the spectrophotometer is only of the

distilled water since the cuvettes are present in both the reference and sample chambers as

equation (1) shows.

2.1.6 Measurement of Corneal Thickness

The thickness of the cornea section and whole cornea is determined, after the

absorbance measurement, through the measurement of the thickness difference of the

sample holder with and without the corneal sample at the room temperature using a

micrometer of 3μm (0.0001 inch) resolution. The micrometer has a ratchet stop

mechanism that enables a consistent application of measuring pressure for each

measurement.

The thickness measured by the micrometer for the cornea sections, used for the UV absorbance measurements, is also verified by the setting of the knife advancement in the microtome. The thickness setting in the microtome can be changed from 2 to 100μm in steps of 2, 4, 6, 8 or 10μm. It is found that the thickness settings of the microtome that are most consistent with the micrometer measurement are around 20 μm. Samples are discarded if the micrometer measurement is different from thickness setting by more than 10μm. The estimated uncertainty in the thickness measurement is less than 20%.

2.2   Part Two

2.2.1   Handling of the Porcine Skin Samples Before and After the Ablation

Fresh porcine skin is obtained from the Department of Comparative Medicine, East Carolina University and Robersonville Meats, Inc. (Robersonville, NC). All skin samples are of fair complexion and removed from the back of the neck of the animals immediately after death and stored on ice until the ablation study. Ablation is performed within 36 hours postmortem. A skin strip of about 10mm wide and 50mm long, with subcutaneous fat removed and hair shaved, is clamped in a sample holder with the surface facing the incoming laser beam. After ablation, the ablated area of the skin sample is immediately trimmed and placed in a fixer to stop the deterioration of the tissue.

2.2.2 Histology Procedures for Ablation Measurement

Three different fixers of ablated skin tissues are tested for the histology analysis:
0.1 M Cacodylate and 2% GAH with a pH of 7.2, Bouins' solution, and 10% buffered
formalin. After fixation, the tissue is prepared for staining. Preparation of the sample
involves dehydration and clearing of the tissue, and infiltrating the tissue with paraffin.
Each of these steps involve precise timing in order to obtain quality sections and reduce
distortion of the ablation cuts, therefore different timing sequences are tested. Once the
tissue is infiltrated with paraffin, then it is embedded in a paraffin block for sectioning
purposes. For sectioning, a microtome (2030 Biocut, Reichert-Jung) is used to section
$10\mu m$ sections of skin. Once the sections are obtained, they are placed on slides and
stained with hemotoxylin and eosin to show better contrast between the epidermis and
subsequent layers of the skin.

2.2.2 Porcine Skin Ablation

A Q-switched Nd:YAG laser (Surelite I, Continuum) is used to generate 8ns
pulses at a wavelength of 1064nm and a repetition rate of 10Hz. The laser pulse energy is
controlled with a half-waveplate and a polarizer beam splitter. The laser beam is focused
on the surface of the skin sample with a single spherical lens. By changing focusing lens
with different focal lengths, we can change the size of the illuminated area on the sample.
The diameter of the focal spot is determined by a knife-edge method. This method
measures the transmitted power of the laser beam as a sharp edge of a translating knife
changes position. During the laser ablation, the sample holder is translated at a constant

speed by a stepping motor to form a linear cut. The skin sample is showered with 0.9%

saline solution every 8 minutes to keep it from dehydration during the ablation. Five to

seven lines, 3mm or 4mm in length, are cut on the skin surface at a specific spot size and

pulse energy. The ablation depth is determined by measuring the depth of the linear cut

of the stained sample under an optical microscope with 5μm resolution. To increase the

sensitivity of measurement of the depth per pulse near the ablation threshold, a large

number of laser pulses is used.

Chapter 3: Experimental Results

3.1 Part One

3.1.1 UV Absorbance Measurements

Figure 7 shows the absorbance of six cornea sections from different porcine

corneas as function of wavelength from 260 to 190nm. One full spectrum of the

absorbance is plotted in the insert of Figure 7 from 350 to 190nm. The absorbance of six

human cornea sections as a function of wavelength from 260 to 190nm is shown in

Figure 8 with one full spectrum from 350 to 190nm displayed in the insert. One of the

human corneas in Figure 8 had been placed in a preservation solution (Optisol, Chiron

Vision) for 1 week before measurement and exhibited a light pink color after it was

removed from the preservation cell. Figures 7 and 8 show that the absorbance readings

have a larger fluctuation in the shorter wavelength region below 195nm than in the longer

wavelength region. This is expected due to the relative large noise presented in the weak

signal caused by the strong absorption of the cornea section and the low light intensity near the shorter wavelength end of the emission spectrum of the light source.

Although the absorbance fluctuates from sample to sample with similar thickness, our measurements clearly indicate that the dependence of the corneal absorption on wavelength is very consistent between 260 and 190nm for both the porcine and human corneas. All the absorbance spectra show that the corneal absorption increases significantly when wavelength decreases from 240 to 220nm. Based on this steep increase, the corneal absorption in the far UV region between 260 and 190nm can be represented by three segments with clear boundaries at 240 and 220nm: a weak absorption segment between 260 and 240nm, a steeply increasing segment between 240 and 220nm, and a high absorption segment below 220nm.

Since the scattering of UV radiation by the cornea is significantly less than the absorption of the UV radiation, we can use Lambert's law to find the transmittance of the corneal sample and the sample holder as:

$$T = \frac{I_o}{I} = (1-R)^2 (1-R')^2 e^{-\alpha d} , \tag{2A}$$

and the transmittance for the sample holder as:

$$T' = \frac{I_o}{I'} = (1-R')^2 , \tag{2B}$$

where we neglect the absorption of the sample holder and I_o and I (or I') are the light intensity at the front and rear surfaces of the sample holder, respectively, R is the Fresnel reflectivity of the glass-cornea interfaces and R' of the air-glass interface (see Fig.4), α is

the linear absorption coefficient of the cornea and d is the thickness of the cornea sample.

The corneal absorbance (A) is obtained by subtracting the absorbance of the sample

holder from the total absorbance of the cornea sample and the sample holder. Therefore,

A is related to T and T' by:

$$A = \log_{10}(\frac{1}{T}) - \log_{10}(\frac{1}{T'}) = 0.434\alpha d - 2\log_{10}(1-R). \qquad (3)$$

If $-2\log_{10}(1-R) << 0.434\alpha d$, then Equation (3) becomes

$$A \cong 0.434\alpha d . \qquad (4)$$

However, the reflection loss contribution to the measured absorbance by R can not be

calculated since the refraction index of the cornea is not known in the far UV region. But

we can estimate that R is smaller than 0.1 in this spectral region from the refraction index

of water since the cornea's major component is water. Thus, Equation (4) should only be

used to accurately calculate the linear absorption coefficient (α) from the measured

absorbance (A) in the segment of strong absorption between 220 and 190nm where the

absorbance measurement is well above 1.0.

In principle, the absorption coefficient α should be measured by finding the slope

of multiple data points from a graph of the absorption as a function of sample thickness

(see Eq. (3)). However, we are unable to measure α in this approach because the

technical difficulty of sectioning the cornea and measuring the absorbance at different

thickness. If the desired thickness is less than 15µm, contiguous sections are hard to

obtain and the variation of section thickness in the light beam area is significant. For a

desired thickness of greater than 30µm, the absorbance A will exceed the maximum scale

of the spectrophotometer. In this limited range of thickness, the slope approach is

statistically unreliable. Instead we choose to calculate the absorption coefficient α by

averaging a large number of data from corneal sections of thickness near 20μm.

Table 1 shows the results of thickness measurements and the calculated α of

porcine corneas, from Equation (4), at four wavelengths of 220, 215, 210, and 193nm.

The linear absorption coefficients α are determined to be 2130 ± 310 (cm^{-1}) at 220nm,

2240 ± 320 (cm^{-1}) at 215nm, 2300 ± 330 (cm^{-1}) at 210m, and 2410 ± 370 (cm^{-1}) at 193nm

from 23 sections out of 18 porcine corneas. Table 2 lists similar results for human

corneas where α is calculated to be 2300 ± 480 (cm^{-1}) at 220nm, 2300 ± 460 (cm^{-1}) at

215nm, 2320 ± 470 (cm^{-1}) at 210nm, and 2340 ± 450 (cm^{-1}) at 193nm from 11 sections

out of 6 human corneas (5 from fresh eye globes and 1 preserved). The standard

deviations in the absorption coefficients for the porcine corneas are consistent with our

expected dominant source of error in the thickness measurement. The large standard

deviations in the linear absorption coefficients for the human corneas may be attributed to

the large statistical fluctuation associated with a relatively small number of samples.

The correlation between the porcine and human linear absorption coefficients at

220, 215, 210, and 193nm is analyzed by the unpaired Student's *t*-test. This test is used

to find a critical value, *t*, for statistical correlation between sets of samples taken

randomly from a population with sizes less than 30 (see Appendix F). The relevant ratio

of *t* for testing the difference between the average linear absorption coefficients of the

porcine corneas and human corneas can be calculated by:

$$t = \frac{(\overline{\alpha}_1 - \overline{\alpha}_2) - (\mu_1 - \mu_2)}{\sqrt{\dfrac{(n_1 - 1)\sigma_1^2 + (n_2 - 1)\sigma_2^2}{n_1 + n_2 - 2}\left(\dfrac{1}{n_1} + \dfrac{1}{n_2}\right)}} \quad , \qquad (5)$$

where $\overline{\alpha}_i$ is the average linear absorption coefficient for our sample of the population i,

n_i is the sample size and $(n_1 + n_2 - 2)$ is the degrees of freedom, σ_i is the standard

deviation of $\overline{\alpha}_i$, and μ_i is the average linear absorption coefficient for the population i.

To test if the average linear absorption coefficients $\overline{\alpha}$ are the same between the sample of

each population, the difference in the population averages is assumed to be zero, which is

referred to as the null hypothesis. By evaluating against the null hypothesis, we are

determining the probability that the sample averages are the same. Once the t ratio is

calculated, it is compared to the table of critical t ratios for a specific confidence level and

the corresponding degrees of freedom. It is found that the calculated t ratio is less than

the critical value of t at the 95% confidence level for the four wavelengths. This indicates

that the null hypothesis is valid and the linear absorption coefficients are equivalent at the

95% confidence level. Therefore, the linear absorption coefficients of the porcine and

human corneas are less than 5% significantly different at each wavelength. Because $\overline{\alpha}_i$ is

determined from a random sampling of the population, we can further suggest that μ_i is

the same value as $\overline{\alpha}_i$.

The effect of freezing on the UV absorbance measurement is investigated through

two sets of tests with the porcine corneas. The absorbance measurement of 3 whole

corneas from 350 to near 290nm is measured before and after freezing. Figure 9 shows

the results from one of the absorbance measurements where the absorbance spectra differs

in the longer wavelength region but converges towards 290nm when the absorbance reading approaches the maximum of the scale. A decrease in corneal thickness is also observed after freezing. The effect of freezing time on the absorbance measurement is also studied with the variation in freezing time from 15 minutes to 10 hours, which is shown in Table 1. There is no significant change found due to the length of freezing time in the spectral region from 260 to 190nm. Because of the technical difficulty in quality sectioning fresh corneas, a direct measurement of the effect of freezing on cornea absorbance in the far UV region is not conducted.

3.1.2 VIS-IR Absorbance Measurements

The VIS-IR absorbance spectra are measured for 3 whole porcine corneas and distilled water. Figure 10 shows the absorbance of one whole porcine cornea as a function of wavelength form 2600 to 600nm which follows the same trend as the other two absorbance spectra. Absorption peaks can be identified at approximately 2440, 1970 and 1420nm which mirror the absorption peaks of distilled water as shown in Figure 11. As the end of the light source's emission spectrum at 2600 nm approaches, a larger fluctuation is seen in the longer wavelength region above 2350nm than in the shorter wavelength region because of the low light intensity.

The effect of freezing on the VIS-IR absorbance measurement is investigated. The absorbance measurement of a whole porcine cornea from 2600 to 600nm is measured before and after freezing. Figure 12 shows the results of the absorbance measurement where a decrease in absorbance is seen from 2440 to 1320nm and an increase from 1320

to 600nm. A decrease in the corneal thickness is found, similar to that observed in the

UV absorbance measurement.

3.2 Part Two

3.2.1 Skin Ablation Study

By experimenting several procedures for porcine skin tissue processing, it is

determined that the Bouins' fixer and the fixer of 0.1 M Cacodylate and 2% GAH with a

pH of 7.2 are time consuming and cause the tissue to become brittle during sectioning.

Therefore, the 10% buffered formalin is chosen to fix the skin tissue immediately after

ablation. Timing for dehydration, clearing and infiltrating the tissue with paraffin is

found to be dependent on the concentration of fat in the porcine skin tissue. Therefore,

the time for each of the steps is increased when the concentration of the fat in the tissue

appears greater. This is estimated visually by the thickness and structure of the tissue.

Following the infiltration process, the procedures for embedding, sectioning, and staining

are standard procedures for histology analysis. A detailed documentation of the

procedures can be found in Appendix E.

Using the histology technique, preliminary results of the laser ablation of fresh

porcine skin tissue are obtained at several spot sizes. We estimate that the error in laser

pulse energy measurements is $\pm5\%$ and that in the depth measurements is $\pm10\%$. The

data obtained from different samples on different days and using a different number of

pulses per spot shows consistency in the measurements confirming that the histology

technique controls the tissue conditions.

Chapter 4: Discussion

4.1 Corneal Absorbance Measurements

Complete far UV absorbance spectra of the cornea and distilled water between 260 and 190nm are measured in this thesis study. The results show that corneal absorption between 260 and 190nm can be divided into three segments with clear boundaries at 240 and 220nm. Also, the average value of the linear absorption coefficient of the cornea sections remains approximately the same as the wavelength decreases from 220 to 190nm. These conclusions confirm a hypothesis based on the analysis of collateral tissue damage zones in the corneal ablation with picosecond laser pulses in the far UV region.[8]

In examining the measurement of the linear absorption coefficient of the cornea at 193nm, it is found that it is about 15% less than that measured by Puliafito *et al.*.[16] Thickness measurements taken of 3 whole porcine corneas show a decrease in the average thickness from 810μm before freezing to 720μm after freezing. This may be attributed to dehydration in the freezing and thawing processes. If a similar reduction in thickness occurred in the cornea sections, the determination of the linear absorption coefficient from the measured absorbance may overestimate the coefficient by about 10%. In addition to the effects of freezing on the absorbance spectra, the porcine eyes obtained from the slaughterhouse are removed from scalded pigs while the porcine eyes used for the last five samples in Table 1 are obtained from the School of Medicine

without scalding. No significant effect due to scalding is found in the measurement of the far UV absorbance of porcine corneas.

The effect of freezing on the absorbance measurement has not been directly studied in the far UV region between 260 and 190nm. Therefore, some uncertainty exists in correlating our results to the clinical investigations of corneal ablation. It is well known that water does not significantly absorb radiation between 193 and 293nm, as our results show in Figure 13, therefore the solid components of the cornea must be responsible for the tissue's absorption.[4] Previous studies indicate that among the major corneal components only collagen has shown a steep rise in the UV absorption spectrum below 240nm,[27] which is also similar to the results reported here. Since small amino acids linked in long molecular chains by peptide bonds compose collagen and freezing only involves the phase transition between water and ice, it is reasonable to assume that freezing has a minimal effect on corneal collagen. Thus, any change in corneal absorption due to freezing may be insignificant compared to the major source of uncertainty in the determination of the sample thickness.

In a previous study on the corneal ablation with short laser pulses in the far UV region, a model is proposed of plasma ablation assisted by chromophore absorption.[8] In this model the threshold of laser ablation of the cornea depends on the linear absorption coefficient of the cornea, nonlinear absorption by water component of cornea and the duration of the laser pulses. It is also suggested that the size of the collateral tissue damage zones is primarily dependent on the linear absorption coefficient of the cornea. Our measurement of the far UV cornea absorption provides an indirect confirmation of

this model. Furthermore, we may conclude that laser pulses with wavelengths in a

"window of ablation" between 220 and 190nm, shown in Figures 7 and 8, can be used for

the surface ablation of the cornea with comparable outcomes.

Spectra of the VIS-IR absorbance of the cornea and distilled water between 2600

and 600 nm are also measured. The large fluctuations on the 1970 nm peak may be due

to an unstable multipot switch on the spectrophotometer. These results are consistent

with the previously reported results.[28] As shown in Figures 10 and 11, the cornea

absorption in this spectral region mirrors that of water where the absorption peaks of

water appear at 1430, 1950, and 2300nm but absorption between them remains low,

which is reasonable since the cornea is composed of 75% water. The difference in the

absorption peak intensity is due to the longer path length of 10mm for the cuvettes

compared to the cornea thickness of ~800μm. Also, the flatness of the absorption peaks

in the distilled water spectrum may be due to the large absorbance reading saturating the

spectrophotometer. In the near future, we plan to extend the measurement of corneal

absorption to the mid-IR wavelength of 3000nm near which the cornea absorbs strongly

again.

The effect of freezing on the absorbance measurement in the VIS-IR spectral

region verifies the previous conclusion that the freezing process has a minimal effect on

the absorbance measurement. The differences in the VIS-IR spectra of porcine corneas

before and after freezing may be attributed to dehydration in the freezing and thawing

processes based on the decrease in thickness from 770μm to 690μm before and after

freezing, respectively. Therefore, it is still reasonable to assume that any change in

corneal absorption due to freezing may be insignificant compared to the major source of uncertainty in the determination of the sample thickness for the UV and VIS-IR absorbance measurements.

4.2 Skin Ablation Study

As a preliminary study for the investigation of the fundamental mechanisms of skin ablation by nanosecond laser pulses at 1064nm, the ablation depth as a function of pulse energy and spot size is measured. The aim is to develop an appropriate histology procedure for the ablation depth measurement that minimizes the interference of artifacts with the ablated tissue conditions. The results obtained from different samples on different days and using a different number of pulses per spot show that the tissue conditions are well controlled through the processing and staining procedures presented in Appendix E.

4.3 Summary

The results presented here are only an initial part of a long-term research project to clearly understand the fundamental mechanisms involved in soft tissue ablation using nanosecond laser pulses. In the near future, we plan to investigate the absorption and scattering of skin tissue in a wide spectral region from 3000 to 190nm, the surface ablation of the cornea and skin tissue by nanosecond laser pulses, and the laser-induced fluorescence spectrum for the corneal and skin tissue ablation. These studies would

provide critical results that are needed to develop a comprehensive model of soft tissue

ablation using nanosecond laser pulses.

Figures
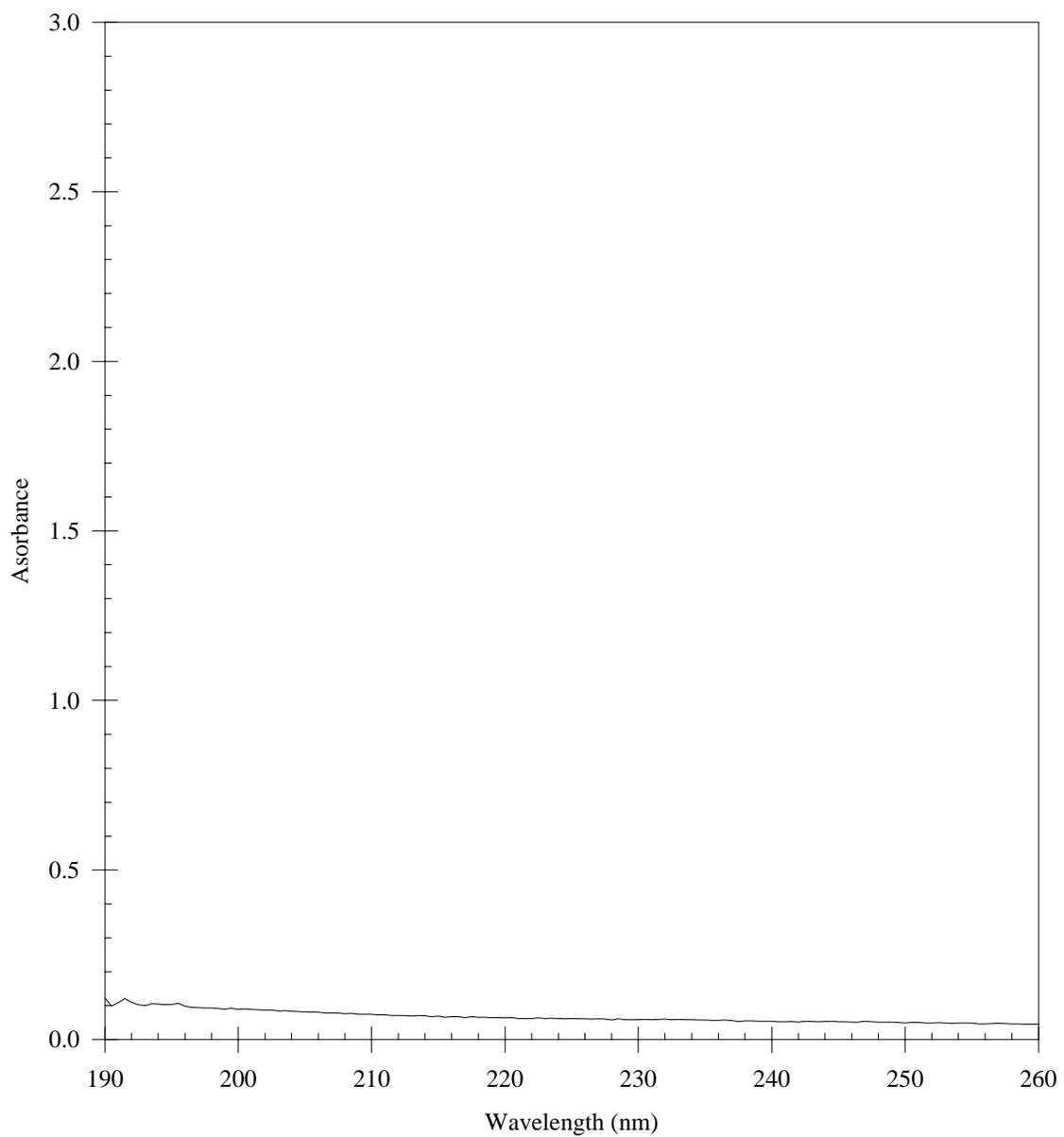
Figure 1: The UV absorbance dependence from 260 to 190nm for the sample holder
made of UV grade fused silica glass with a total thickness of ~12mm and the
two sample and reference apertures of 4mm in diameter to collimate the
incident and transmitted beams.

PIECE 1

● holes drilled and tapped for 2-56 screws

Side View

Inside View

0.050″

2.40″

0.250″

0.450″

0.100″ 0.100″

1.30″

0.100″ 0.100″

0.100″

0.500″
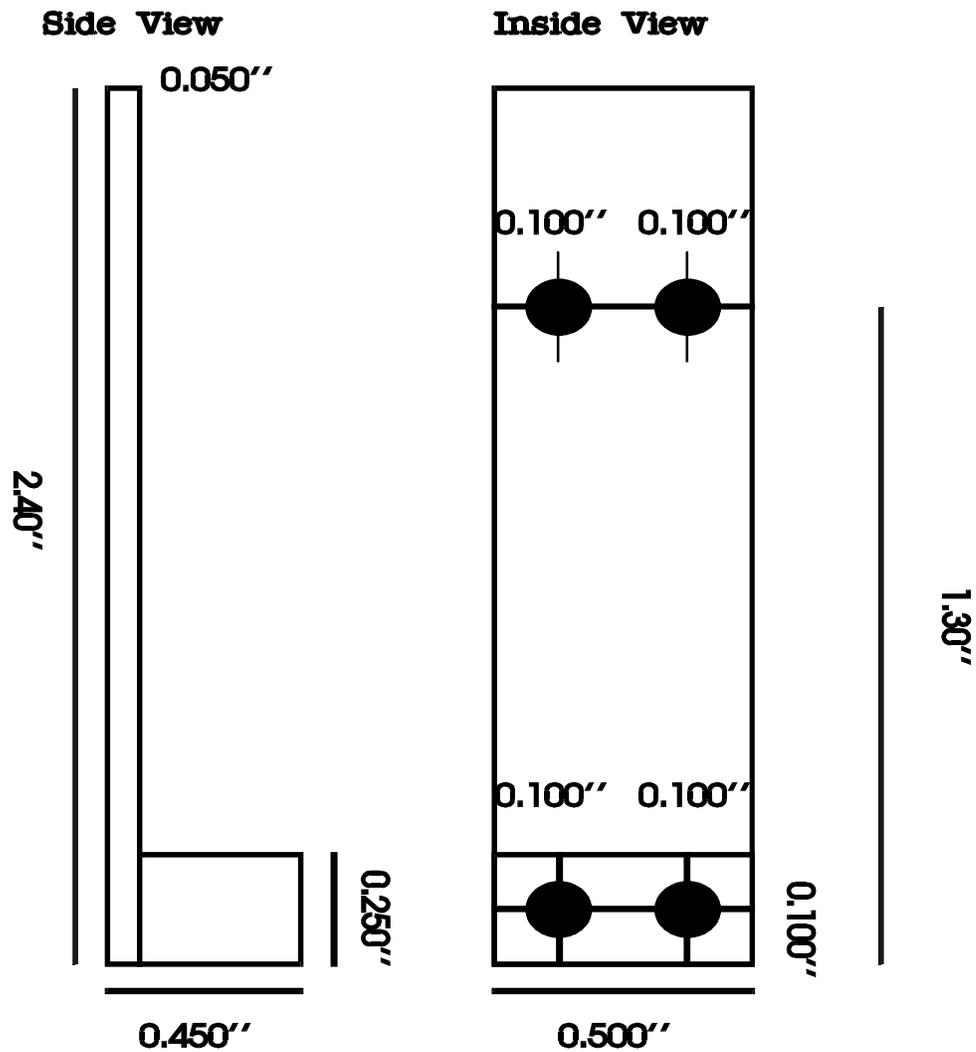
Figure 2: The design of piece 1 of the holder to clamp the two rectangular optical windows used for the sample holder in the sample chamber.

PIECE 2

● holes drilled and tapped for 2-56 screws

Side View   **Inside View**
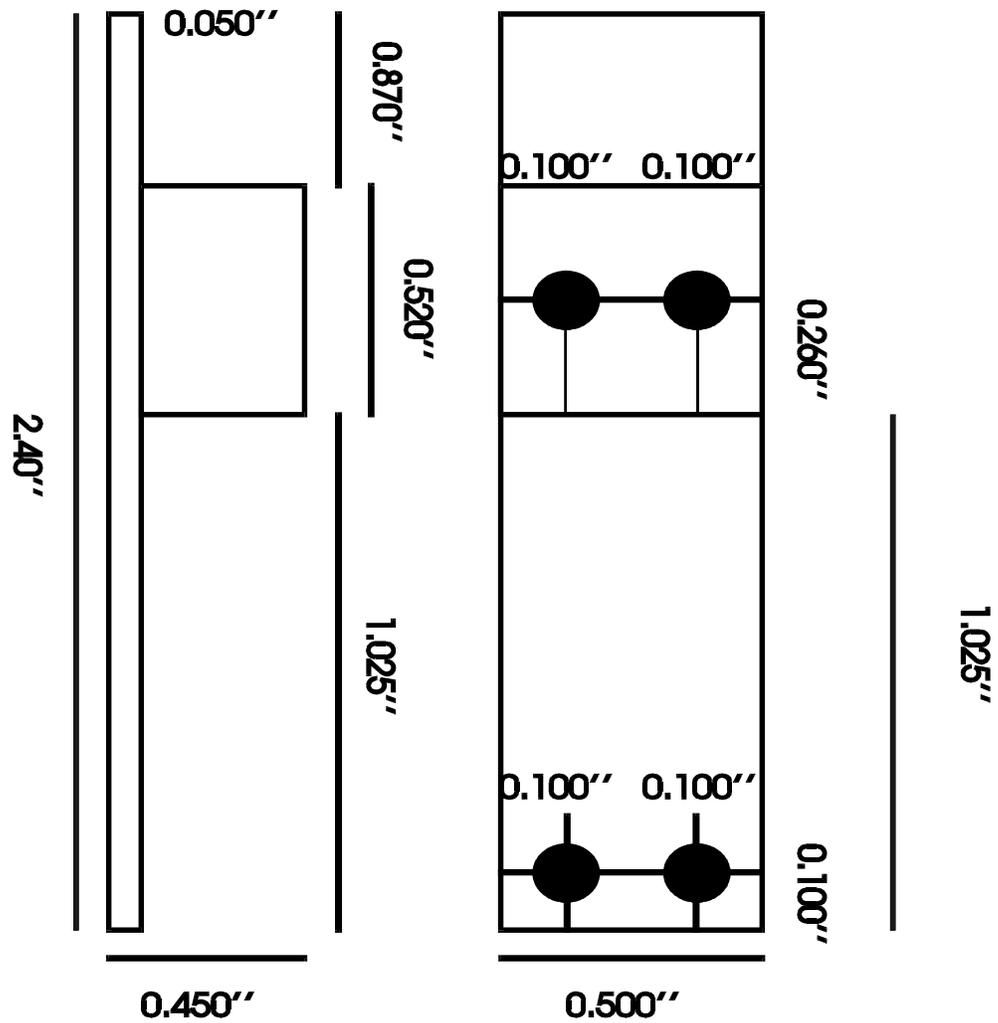
Figure 3: The design of piece 2 of the holder to clamp the two rectangular optical

widows used for the sample holder in the sample chamber.

Glass ☐ and Cornea ☐
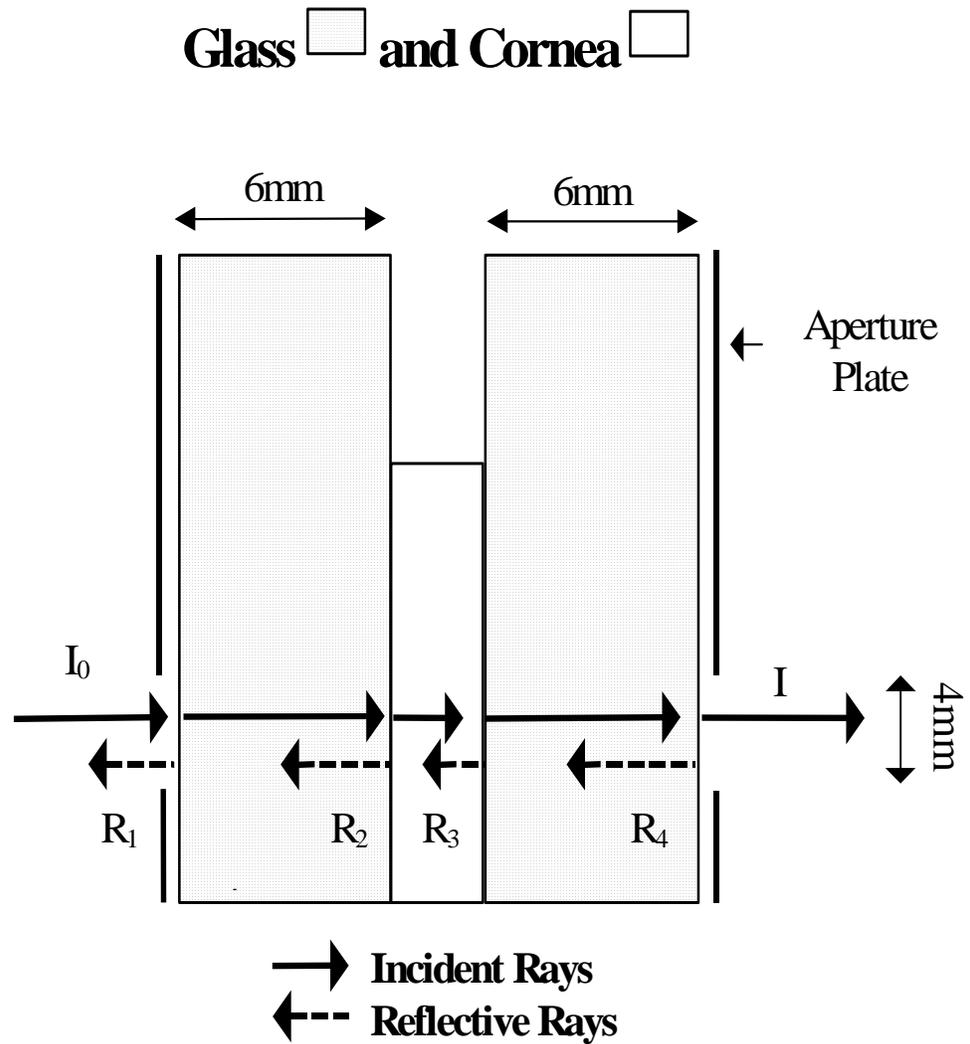
Figure 4: The configuration of the sample holder, cornea section and aperture plates.
The incident ray (I_0) is reflected at the four interfaces with $R_2 = R_3 = R$ and
$R_2 = R_4 = R'$. The reflected rays are translated for a clear view.
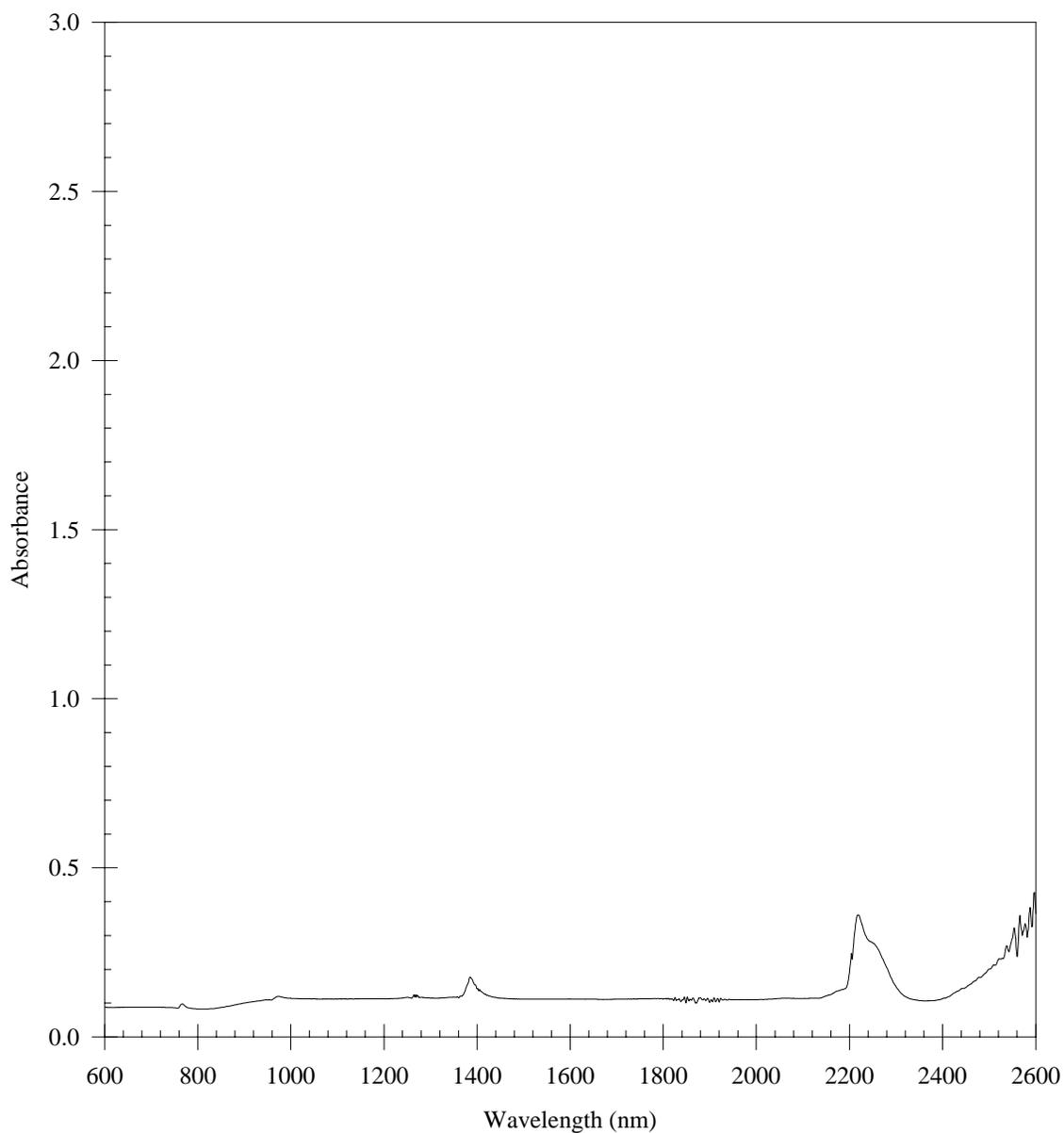
Figure 5: The VIS-IR absorbance dependence from 2600 to 600nm for the sample holder

made of UV grade fused silica glass with a total thickness of ~12mm with the

two sample and reference apertures of 4mm in diameter to collimate the

incident and transmitted beams.

Spectrophotometer Optical System

(Model 17D, Varian Associates)

Cell Compartments

Reference

Lamp → Monochromators and Rotating Mirror

Sample

Detector and Electronics → PC
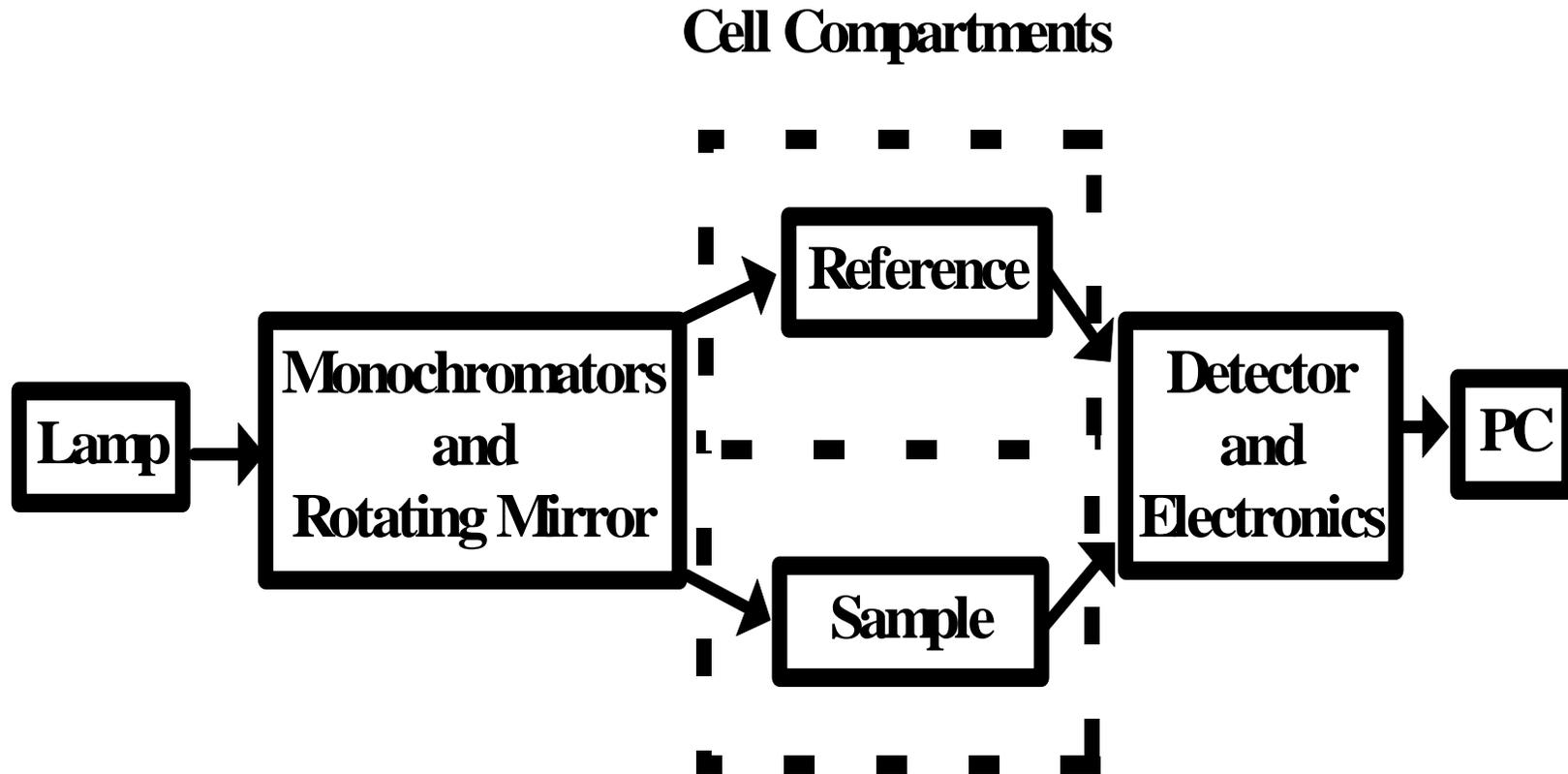
Figure 6: The schematic for the dual-beam UV-VIS-IR spectrophotometer (Model 17D, Varian Associates).
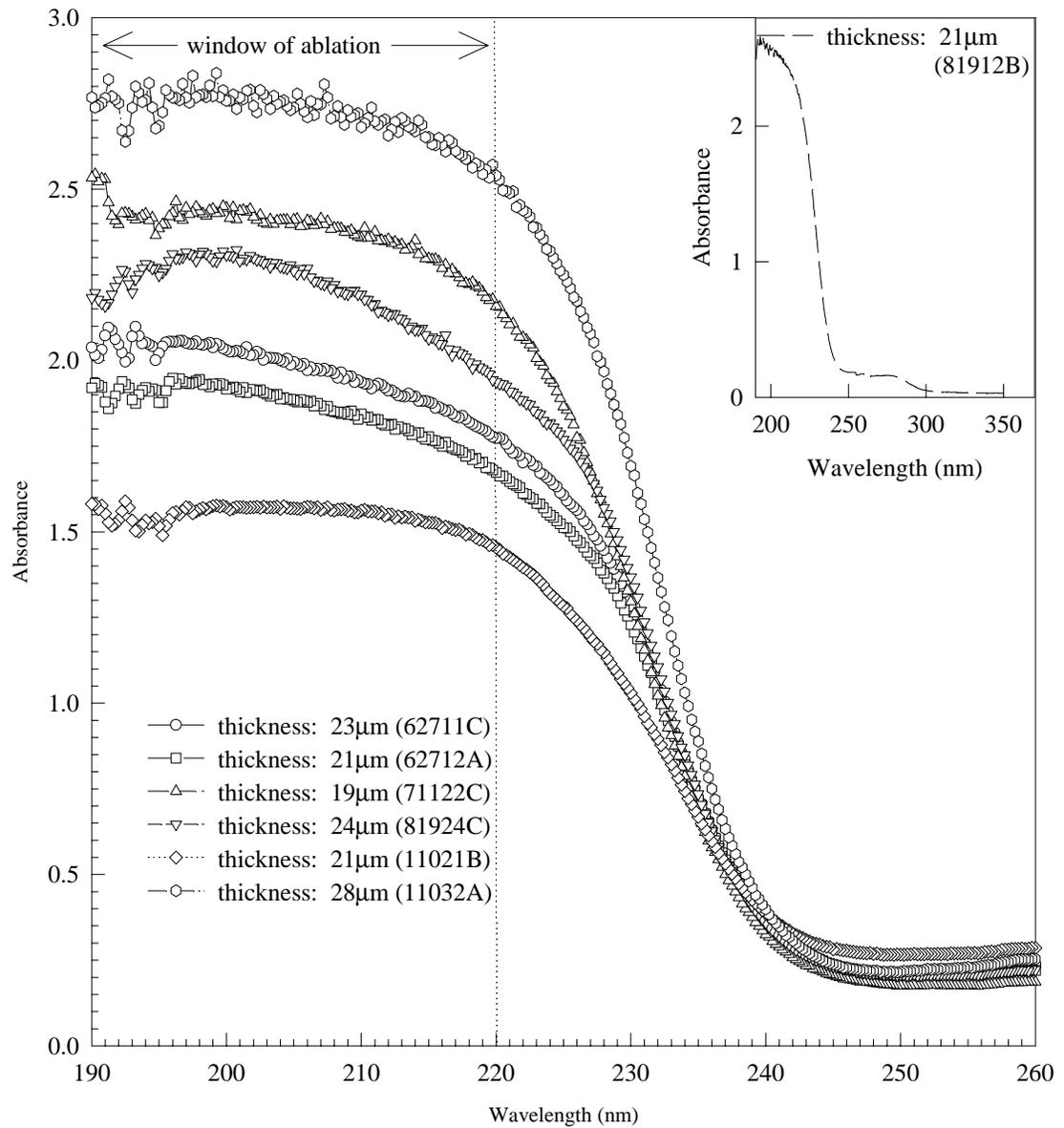
Figure 7: The UV absorbance dependence on the wavelength for six porcine cornea sections from six porcine corneas between 260 to 190nm with the two sample and reference apertures of 4mm in diameter. Insert: The absorbance for one porcine cornea section between 350 to190nm.
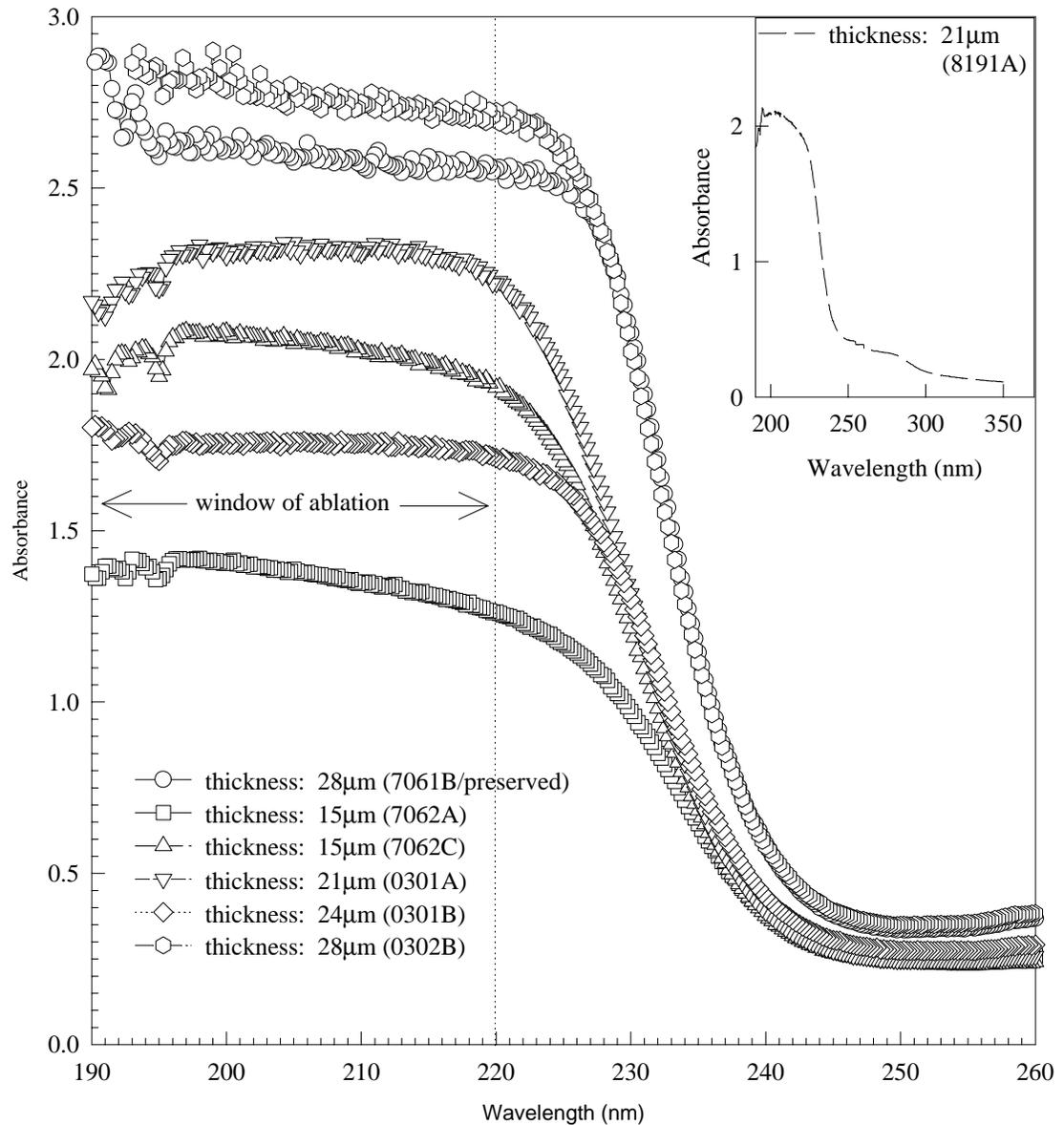
Figure 8: The UV absorbance dependence on the wavelength for six human cornea
sections from four human corneas (three fresh and one preserved) between 260
and 190nm with the two sample and reference apertures of 4mm in diameter.
Insert: The absorbance for one human cornea section between 350 to 190nm.

Table 1: The thickness and linear absorption coefficients of porcine cornea sections

calculated at 220, 215, 210, and 193nm using equation (4).

sample #	thickness (μm)	α (cm^{-1}) at 220 nm	α (cm^{-1}) at 215 nm	α (cm^{-1}) at 210 nm	α (cm^{-1}) at 193 nm	postmortem* / freezing time (hour)
62711b	20	2230	2290	2350	2430	1.5 / 1.2
62711c	23	1820	1940	2010	2120	1.5 / 9.0
62712a	21	1820	1930	1990	2120	1.3 / 1.5
62731b	25	1700	1760	1790	2080	3.3 / 3.2
71121a	26	2490	2510	2590	2290	5.2 / 0.6
71122c	19	2680	2880	2940	3010	7.2 / 5.6
71131a	27	1850	1910	1970	1940	7.2 / 7.5
72911a	18	2030	2180	2340	2510	1.5 / 0.3
72911b	18	2330	2410	2520	2670	1.5 / 10.5
72912a	26	2130	2290	2350	2630	2.4 / 0.4
72912b	23	2360	2520	2580	2680	2.4 / 1.2
72923a	21	2030	2140	2140	2260	5.2 / 0.7
72936a	12	2630	2710	2710	2630	9.0 / 0.7
81923a	15	2430	2640	2700	3180	5.6 / 1.0
81912b	21	2450	2620	2750	2910	2.8 / 2.8

81923b	20	2070	2330	2480	2800	5.2 / 2.0
81924b	21	1800	1900	1930	2100	7.6 / 5.0
81924c	24	1910	2030	2130	2190	7.6 / 5.9
11011a	30	2090	2170	2190	2160	2.0 / 0.5
11021b	21	1610	1680	1710	1660	4.3 / 1.5
11022a	15	2570	2590	2600	2510	4.3 / 2.7
11031a	16	1960	2000	2020	2220	6.8 / 1.2
11032a	28	2090	2180	2230	2280	6.8 / 2.2

* The postmortem time is defined to be the period between animal death and the

beginning of corneal freezing.

Table 2: The thickness and linear absorption coefficients of human cornea sections

calculated at 220, 215, 210, and 193nm using equation (4).

sample #	thickness (μm)	α (cm^{-1}) at 220 nm	α (cm^{-1}) at 215 nm	α (cm^{-1}) at 210 nm	α (cm^{-1}) at 193 nm	postmortem time
7061a	19	2590	2680	2750	2920	1 week (preserved)
7061b	28	2080	2090	2090	2180	1 week (preserved)
7062a	15	1970	2030	2030	2120	33 hours
7062b	20	1600	1660	1670	1720	33 hours
7062c	15	3000	3180	3210	3140	33 hours
8191a	17	2710	2740	2760	2680	28 hours
8192a	21	2920	2290	2250	2120	30 hours
0301a	21	2450	2530	2540	2420	28 hours
0301b	24	1650	1680	1680	1680	28 hours
0302a	21	2090	2160	2220	2390	28 hours
0302b	28	2260	2260	2290	2380	28 hours
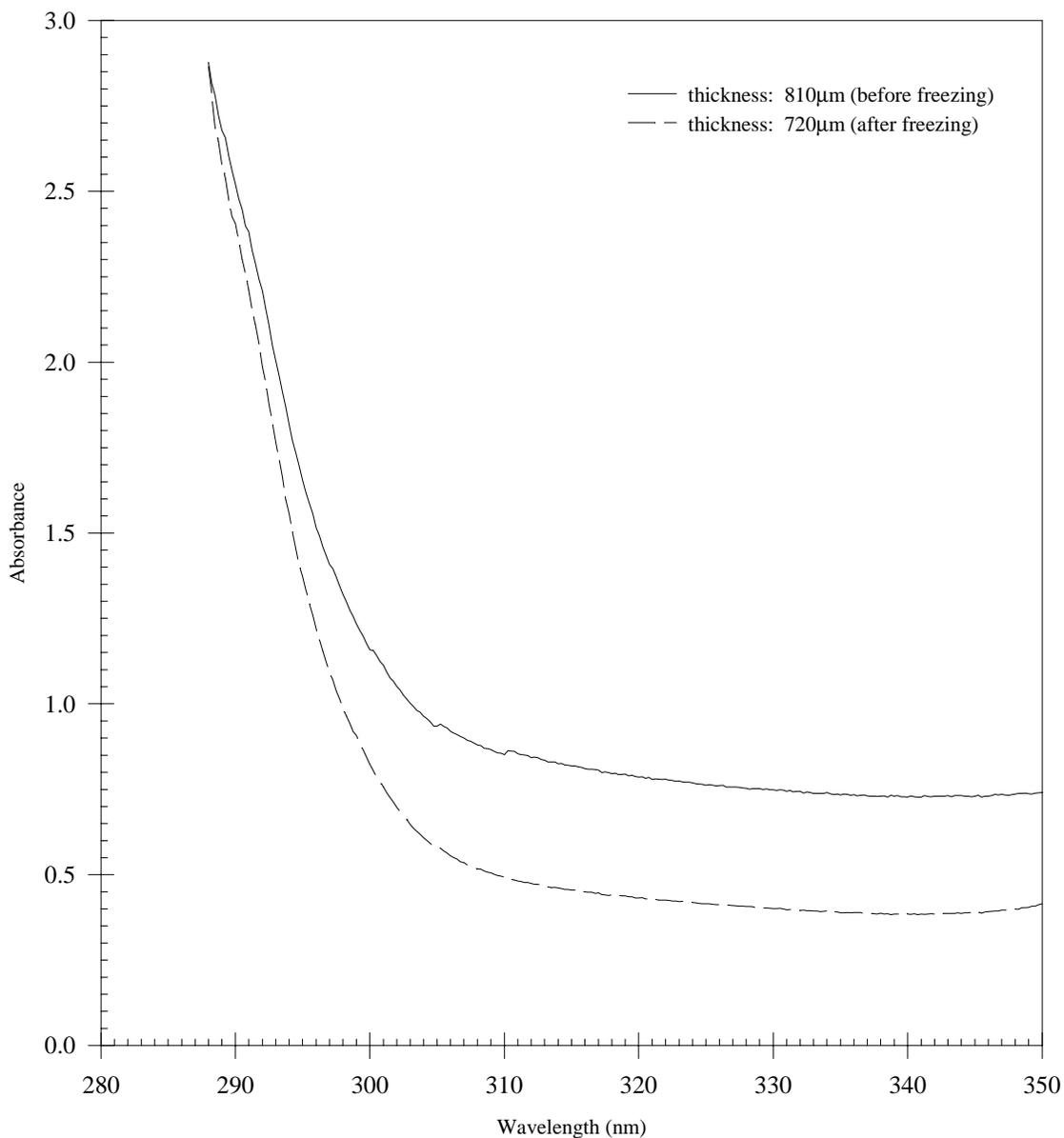
Figure 9: The UV absorbance dependence on wavelength from 350 to near 290nm of one

whole porcine cornea before and after freezing. The two apertures of 4mm in

diameter are present in both chambers to collimate the incident and transmitted
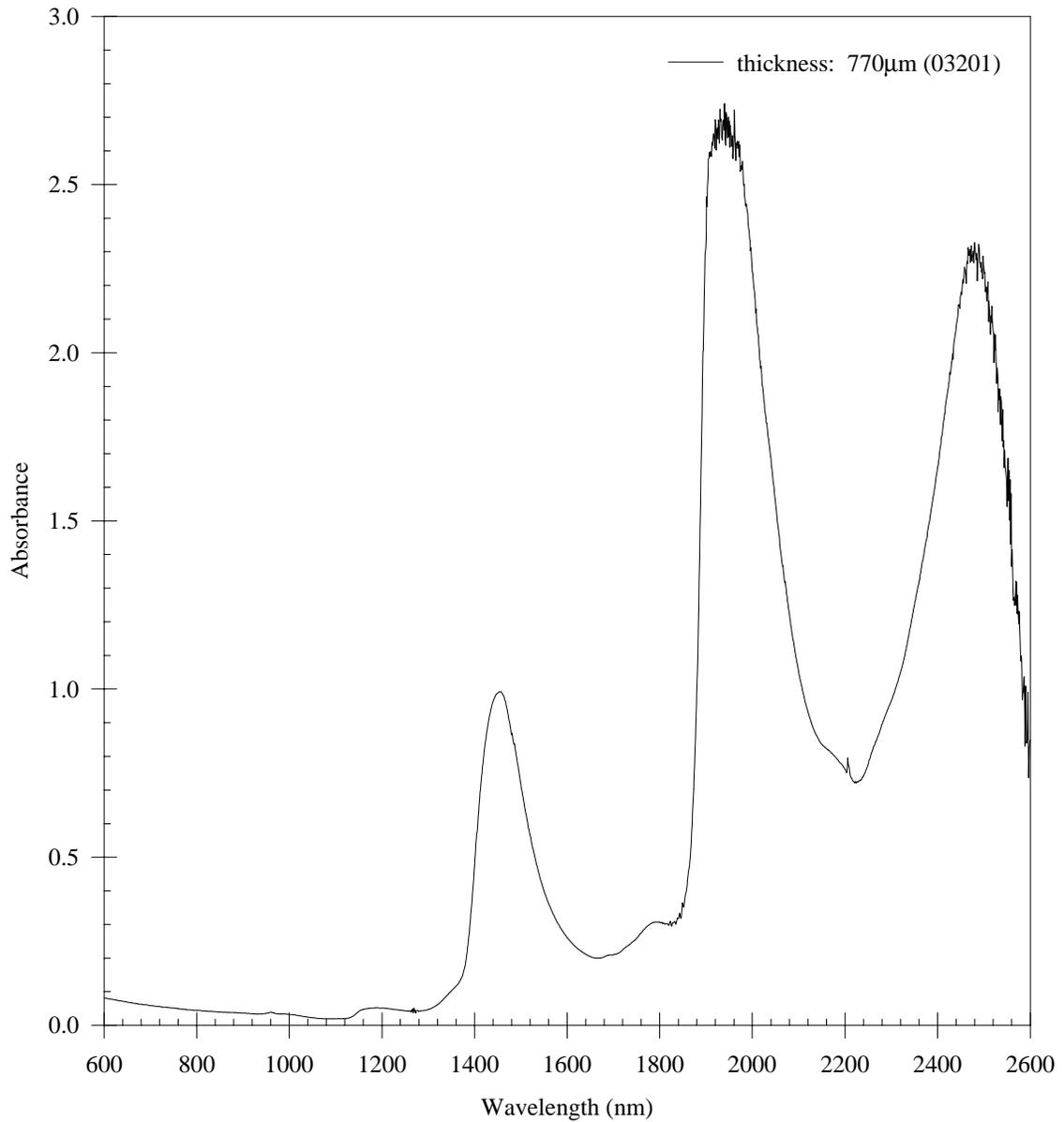
beams.

Figure 10: The VIS-IR absorbance dependence on wavelength for a porcine cornea between 2600 to 600nm. The two apertures of 4mm in diameter are present in both chambers to collimate the incident and transmitted beams.
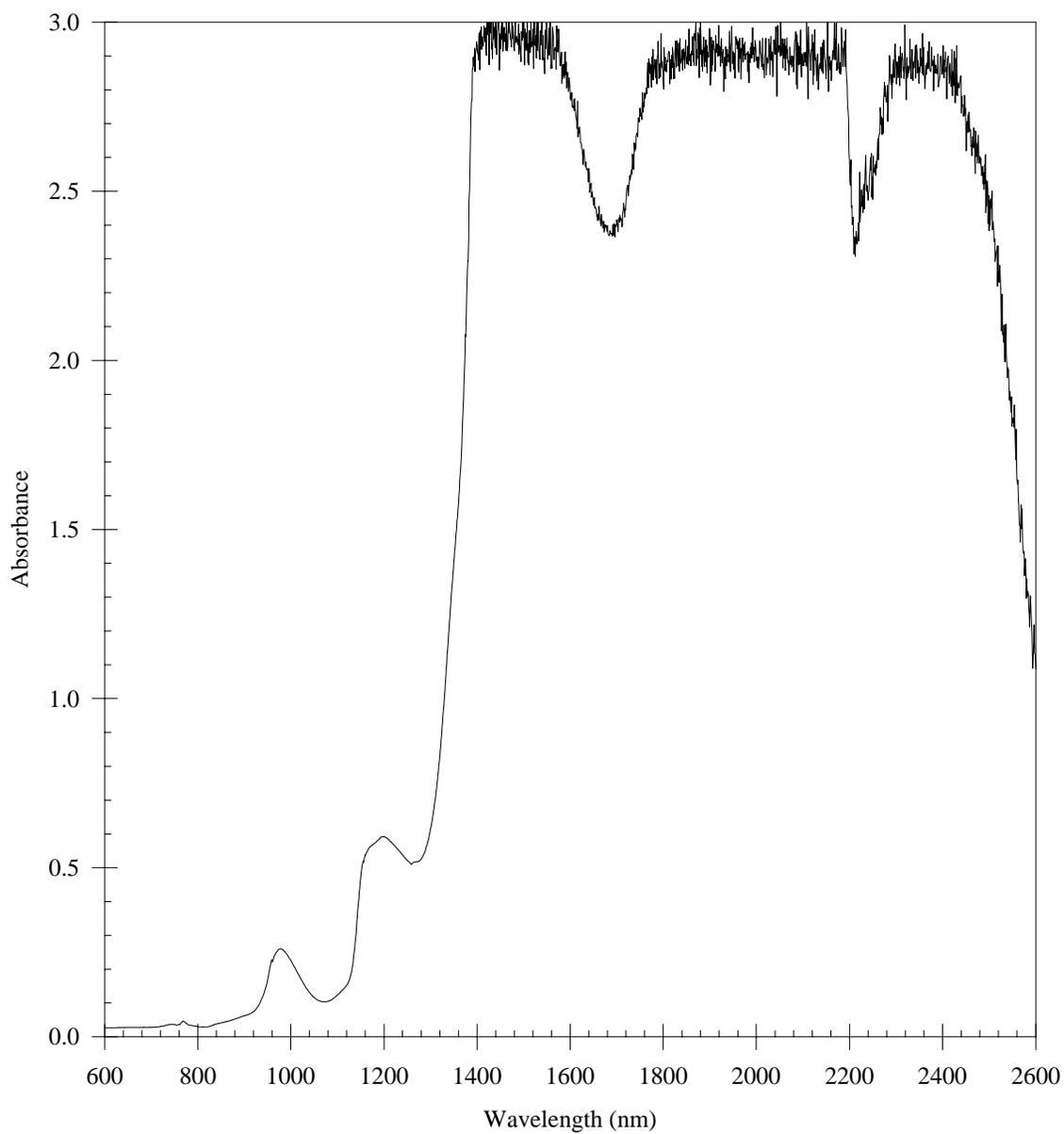
Figure 11: The VIS-IR absorbance dependence on wavelength for distilled water from 2600 to 600nm with a path length of 10mm and the two apertures of 4mm in diameter in both chambers to collimate the incident and transmitted beams.
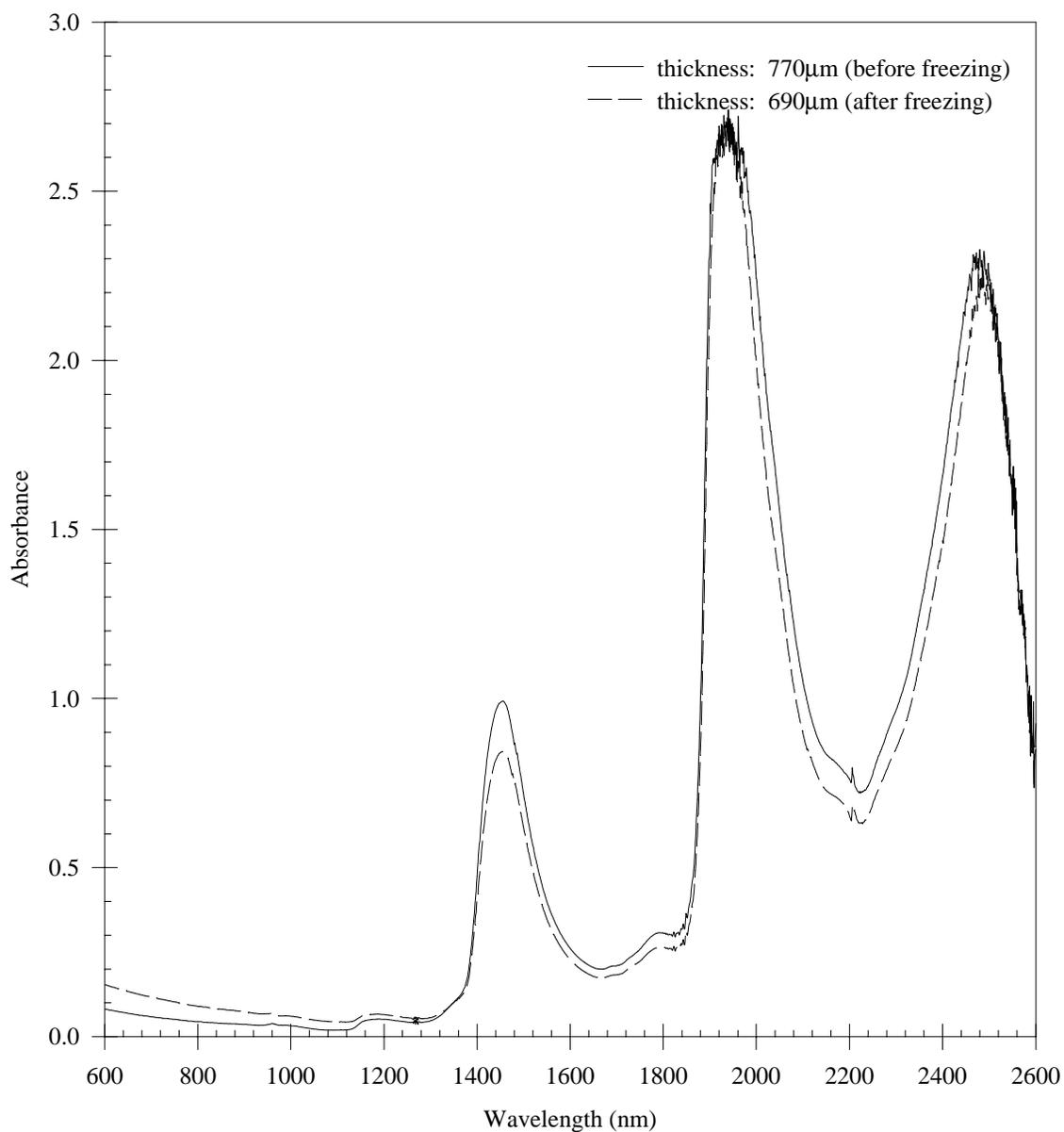
Figure 12: The VIS-IR absorbance dependence on wavelength from 2600 to 600nm of one whole porcine cornea before and after freezing. The two apertures of 4mm in diameter are present in both chambers to collimate the incident and transmitted beams.
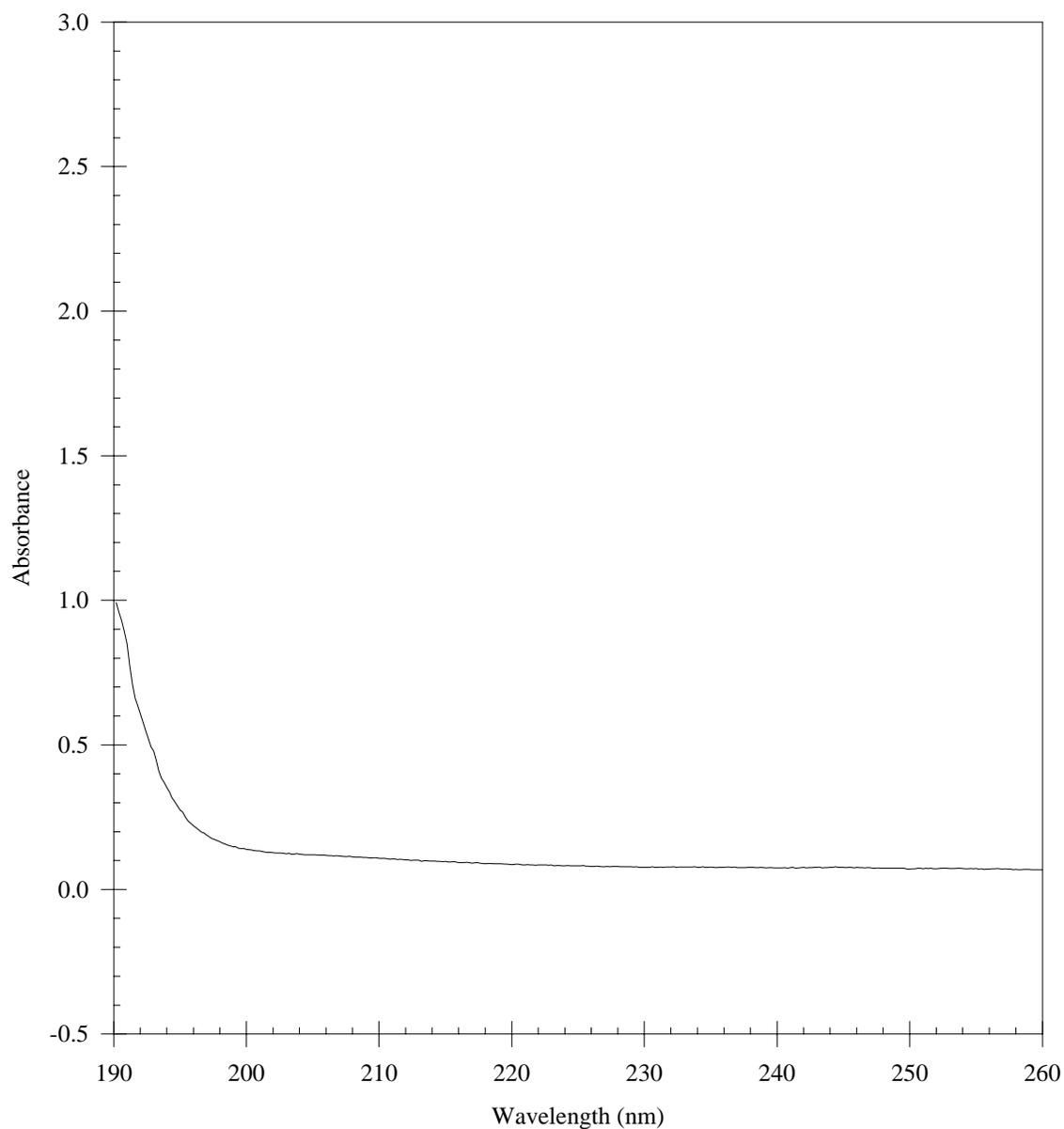
Figure 13: The UV absorbance dependence on the wavelength for distilled water from
260 to 190nm with a path length of 10mm without the two apertures of 4mm
in diameter in both chambers in order to increase the signal strength for the
absorbance measurement.

References

1   Siegman AE, *Lasers,* Mill Valley, CA: University Science Books, 1986

2   Berns MW, "Laser surgery", *Scientific American*, :84-90, June 1991

3   Thomsen S, "Pathologic analysis of photothermal and photomechanical effects of laser-tissue interactions", *Photochem. Photobio.*, **53**:825-835, 1991

4   Krauss JM, Puliafito CA, "Lasers in Ophthalmology", *Lasers Surg. Med.*, **17**:102-159, 1995

5   Anderson RR, Parrish JA, "Selective photothermolysis: precise microsurgery by selective absorption of pulsed Radiation", *Science*, **220**:524-527, 1983

6   For review see, Welch AJ, Motamedi M, Raasteger S, LeCarpentier GL, Jansen D, "Laser thermal ablation", *Photochem. Photobio.*, **53**:815-823, 1991 and references therein

7   Fuhimoto JG, Linn WZ, Eppen EP, Puliafito CA, Steinert RF, "Time-resolved studies of Nd:YAG laser induced breakdown: plasma formation, acoustic wave generation, and cavitation", *Invest. Ophthalmol. Vis. Sci.,* **26**:1771-1777, 1985

8   Hu XH, Juhasz T, "Study of corneal ablation with picosecond laser pulses at 211nm and 263nm", *Laser Surg. Med.*, **18**:373-380, 1996

9   Srinivasan R, Sutcliffe E, "Dynamic of the ultraviolet laser ablation of corneal tissue", *American Journal of Ophthalmology*, **103**:470-471, 1987

10   Steinert RF, Puliafito CA, Trokel S: "Plasma formation and shielding by three ophthalmic Nd:YAG lasers, *Am. J. Ophthalmol.,* **96**:427-434 (1983)

11   Vogel A, Schwelger P, Frieser A, Asiyo MN, Birrngruber R, "Intraocular Nd:YAG laser surgery: light-tissue interaction, damage range, and reduction of the collateral effects", *IEEE J. Quan. Electron.*, **26**:2240-2260 (1990)

12   Ediger MN, Petit GH, Weiblinger RP, Chen CH, "Transmission of corneal collagen during ArF excimer laser ablation", *Lasers Surg. Med.*, **13**:204-210, 1993

13   Watanabe S, Flotte TJ, McAuliffe DJ, Jacques SL, "Putative photoacoustic damage in skin by pulsed ArF excimer laser", *J. Invest. Dermatol.*, **90**:761-766, 1988

14 Tuft S, Al-Dhahir R, Dyer P, Zhu ZH, "Characterization of the fluorescence spectra produced by excimer laser irradiation of the cornea", *Invest. Ophthalmol. Vis. Sci.*, **31**:1512-1518, 1990

15 Ediger MN, "Excimer-laser-induced fluorescence of rabbit cornea: radiometric measurement through the cornea", *Lasers Surg. Med.*, **11**:93-98, 1991

16 Puliafito CA, Steinert RF, Deutsch TF, Hillenkamp F, Dehm EJ, Adler CM, "Excimer laser ablation of cornea and lens", *Ophthalmology*, **92**:741-748, 1987

17 Trokel SL, Srinivasan R, Braren B, "Excimer laser surgery of the cornea", *Amer. J. Ophthalmology*, **96**:710-715, 1983

18 Krueger RR, Trokel SL, Schubert HD, "Interaction of ultraviolet laser light with the cornea", *Inv. Ophthalmol. Vis. Sci.*, **26**:1455-1464, 1985

19 Ren Q, Galilitis RP, Thompson KP, Lin JT, "Ablation of the cornea and synthetic polymers using a UV (213nm) solid state laser", *IEEE J. Quan. Electron.* **26**:2284-2288, 1990

20 Mitchell J, Cenedella RJ, "Quantitation of ultraviolet light absorbing fractions of the cornea", *Cornea*, **14**:266-272, 1995

21 Krauss JM, Puliafito CA, Steinert RF, "Laser interaction with the cornea", *Surv. Ophthalmol.,* **31**:37-53, 1986

22 Wheeland RG, "Clinical uses of lasers in dermatology", *Lasers Surg. Med.*, **16**:2-23, 1995

23 Mackenzie IC, "Ordered structure of the epidermis", *J. Invest. Dermatol.,* **65**:45-51, 1975

24 Kligman AM, "The biology of the stratum corneum", *In* Lobitz WC Jr, Montagna W, eds. *The Epidermis*, New York: Academic Press, 1964

25 Lavker RM, Dong G, Zheng P, Murphy GF, "Hairless micropig skin: a novel model for studies of cutaneous biology", *American Journal of Pathology*, **138**:687-697, 1991

26 Bartell TH, Mustoe TA, "Animal models of human tissue expansion", *Plast. Reconstru. Surg.,* **83**:681-686, 1989

27   Loofbourow JR, Gould BS, Sizer IW, "Studies on the ultraviolet absorption of collagen", *Arch. Biochem.*, **22**:406-411, 1949

28   Boettner EA, Wolter JR, "Transmission of the ocular media", *Investigative Ophthalmology*, **1**:776-783, 1962

29   Lab Tek Products, *Operating Manual: Tissue-Tek microtome-cryostat*, Naperville: Lab Tek, 1974

30   Varian Associates, *Operating Manual: model 17D spectrophotometer system*, Palo Alto: Varian

31   Brown GG, *An introduction to histotechnology*, New York: Appleton-Century-Crofts, 1978.

32   Preece A, *A manual for histologic technicians, 3rd ed.*, New York: Churchill/Livingston, 1972

33   Kachigan SK, *Statistical analysis: an interdisciplinary introduction to univariate and multivariate methods*, New York: Radius Press, 1986

34   Milewski EG, *The essentials of statistics II*, New Jersey: REA, 1994

Appendix A: Cornea Sectioning

While preparing to study the absorption properties of the cornea, the challenge is to design a sectioning procedure that preserves the absorption properties of the cornea. A frozen sectioning method is chosen due to two advantages. First, there is the absence of fixing agents that may distort tissue properties. Second, the duration of time before examination of the section is greatly reduced. This is a supplement to the operating manual[29] for the Ames Tissue-Tek® Microtome /Cryostat: Microtome model no. 4551 and Cryostats nos. 4550 115 VAC/60HZ and 4552 220 VAC/50Hz. The procedure is designed to slice 10 to 40µm contiguous sections of cornea in steps of 10µm while frozen in a freezing preservation medium (OCT).

The advances in frozen sectioning developed from practice rather than theory making the process an art before a science. There are many critical factors that effect the quality of the slices attained. The tissue, knife, and tools must be maintained at a correct temperature. If the temperature of the tissue is too low, the sections may crumble during sectioning. In contrast, if the temperature is too high, the tissue and the OCT will not remain frozen during sectioning. The optimal temperature of the tissue for sectioning the cornea is approximately - 18°C. Likewise if the knife temperature is too high, the sections may adhere to the knife making it difficult to transfer the section to the sample holder. The knife's sharpness and angle are also of critical importance. A dull, dirty knife may tear the sections during the sectioning process. An improper knife angle may cause tissue scraping, inconsistencies of section thickness, and also tearing of the section

during sectioning. The operating manual[29] recommends a 5° angle, but experience and personal preference will produce better sections. Also, the motion of turning the hand wheel during the sectioning of the cornea will effect the quality of the sections obtained. In order to obtain a contiguous section with uniform thickness, the hand wheel must be turned with a fluid motion at approximately a constant rate for every section.

The following procedure mirrors the operating manual[29] to an extent. The additions are developed from trial and error.

A.1 Preparing the Cryostat-Microtome

1. The microtome-cryostat is cleaned from debris. All the movable parts are lubricated with oil for better fluid motion while sectioning.

2.   All tools, including the specimen blocks, used for the sectioning process are cleaned and placed in the cryostat.

3. The knife is sharpened and placed in the cryostat and the knife advancement set to 10μm.

4. The cryostat is set at -18°C and allowed to cool for at least 12 hours before sectioning takes place.

A.2 Preparing the Specimen Blocks

1. The specimen block is removed form the cryostat and its face warmed by rubbing it with a finger which allows the OCT to adhere better to the specimen block and prevents slippage during sectioning.

2. Enough OCT is placed on the specimen block to form a platform. The specimen block is returned to the freeze bar to allow the OCT to freeze. (Freezing is complete when the OCT turns solid white.)

3. The specimen block is mounted in the chuck of the microtome and the chuck tightened to secure the specimen block in the uppermost position.

4. The knife's edge is brought close to the frozen OCT platform by turning the gross adjusting wheel clockwise. Then the hand wheel is turned to slice the OCT until a large enough surface area results to occupy the cornea specimen.

5. The plate-type anti-roll device is lowered onto the knife to determine if the sections will lay flat on the knife. The hand wheel is turned to obtain a section. If the section does not lay flat on the knife, the plate-type anti-roll device is adjusted so that it is parallel with the knife's edge. The sectioning process is repeated until the section of OCT lays flat on the knife.

6. The specimen block is removed from the chuck and returned to the freeze bar.

A.3 Preparing the Cornea for Sectioning

1. The cornea is prepared by rinsing any excess viscous fluid from it with saline. This helps the cornea remain embedded in the OCT during sectioning.

2. The specimen block is removed from the freeze bar and placed outside the cryostat.

3. The cornea is placed, as flat as possible so no air will be trapped between the cornea and the OCT, over the surface area of the OCT platform. The entire cornea is then covered with OCT.

4. The specimen block is then returned to the freeze bar to allow the cornea to freeze for 15 minutes or longer. (Freezing is complete when the OCT is solid white.)

5. Once frozen, the specimen block is mounted in the chuck of the microtome and the chuck tightened to secure the specimen block in the uppermost position.

A.4 Sectioning the Cornea

1. The knife's edge is retreated by rotating the gross adjusting wheel counterclockwise until the knife's edge is just above the OCT. The hand wheel is turned to section the OCT until the cornea is reached. This is apparent when a yellowish discoloration appears representing the cornea specimen.

2. Slicing is continued until a full section of the corneal stroma (position dependent on species of cornea), without holes or tears, appears with the desired surface area.

3. All debris is cleared away from the knife and plate-type anti-roll device.

4. The plate-type anti-roll device is lowered onto the knife.

5. The hand wheel is turned to obtain the desired thickness of the cornea section. Since the knife advancement is set at 10μm, the hand wheel is turned clockwise until the section is almost sliced and then back counterclockwise to obtain a 20μm section.

The knife is advanced immediately before sectioning, so rotating the hand wheel in this manner advances the knife twice, 20μm, before the section is sliced.

6. The cornea section is allowed to remain on the knife for a few seconds to allow the section to recool before transferring to the sample holder.

A.5 Transferring the Cornea Section to the Sample Holder

1. The optical window of the sample holder is cleaned thoroughly with acetone and placed at room temperature.

2. The plate-type anti-roll device is lifted from the knife.

3. The optical window is placed directly above the cornea section, so that the cornea section is directly below the exact desired position on the optical window.

4. The optical window is then lowered to barely touch the cornea section.

5. Once the cornea section adheres to the optical window, the optical window is removed from the cryostat and allowed to return to room temperature. The cornea section is then clamped between the two optical windows forming the sample holder.

Appendix B: Calibration of the Spectrophotometer

B.1 Cleaning

The lenses and mirrors are cleaned with acetone and the optical compartment is purged for 15 minutes with nitrogen at 1.5 l/min.

B.2 Zero T Check (refer to Section 1.6 pp. 1-44)[30]

B.2.1 For UV-VIS Detector

With the detector set on UV-VIS, the Absorbance Drift Test Switch is set to Absorbance Drift (the out position) giving an absorbance reading of +0.0005. Then the Absorbance Drift Test Switch is set to Operate (the in position) giving an absorbance reading of +0.0000.

B.2.2 For IR Detector

With the detector set on IR, the Absorbance Drift Test Switch is set to Absorbance Drift (the out position) giving an absorbance reading of -0.0005. Then the Absorbance Drift Test Switch is set to Operate (the in position) giving an absorbance reading of $\pm$0.0100.

Since the absorbance readings are greater than $\pm$0.0004 for both the UV-VIS and IR detectors, the adjustment procedure is followed in Section 13.5.4.6.1 pp. 13-57 in the

spectrophotometer's manual.[30] Once the procedure is finished, then the Zero T Check is repeated.

B.2.3 For UV-VIS Detector

With the detector set on UV-VIS, the Absorbance Drift Test Switch is set to Absorbance Drift (the out position) giving an absorbance reading of +0.0001. Then the Absorbance Drift Test Switch is set to Operate (the in position) giving an absorbance reading of +0.0000.

B.2.4 For IR Detector

With the detector set on IR, the Absorbance Drift Test Switch is set to Absorbance Drift (the out position) giving an absorbance reading of 0.0000. Then the Absorbance Drift Test Switch is set to Operate (the in position) giving an absorbance reading that fluctuates between ±0.0005.

B.3 Checking the Wavelength Counter versus Time

The Wavelength Scan Speed is set at 0.5nm/sec and the time is taken with a stopwatch every 10nm. A consistent change in time is seen as the wavelength scanned which shows linearity in the scan speed. The test is repeated for a Wavelength Scan Speed of 0.1nm/sec and shows the same result.

B.4 Checking the Relationship Between the Spectrophotometer's Digital Display and the Computer Reading

The wavelength is set at 550nm and the Slit Knob at 3.0. In order to change the Digital Display reading, the Balance is adjusted and various colored filters are placed in the sample chamber to obtain a higher absorbance. The graph of the Computer Reading versus the Digital Display shows a 1:1 ratio between the two readings.

B.5 Starting and Warm-up of Spectrophotometer

The spectrophotometer is turned on and set at the settings that will be used during the scan as described on pp. 5-7 of the spectrophotometer's manual.[30] It is important to allow the spectrophotometer to warm-up for at least one hour at the initial settings before any measurements are taken. This allows for the electronics to come to an operating temperature.

B.6 Zero Absorbance Baseline for UV, VIS, and IR Wavelengths

In order to have a zero reading without a sample, the spectrophotometer has to be calibrated to eliminate very slight differences in beam geometry that can cause the zero absorbance to vary from one wavelength to another. The spectrophotometer has a multiple potentiometer (Multipots) systems that may be adjusted to eliminate such variations from the measurement of zero absorbance level. The procedure used to straighten and zero the baseline is on pp. 5-23 of the spectrophotometer's manual.[30] This

procedure is completed for all wavelengths and the baselines are graphed for reference (Figures B.1-B.3).

B.7 Testing the UV Absorbance Reading Using a Standard Dye Solution

The UV absorbance reading is tested using a standard dye (Epolite® 111-125) which has a maximum wavelength of 949nm following the procedure on pp. 4-1 of the spectrophotometer's manual.[30] An absorbance spectrum of a dye concentration of 3mg/l is provided by the manufacturer from 1450 to 350nm. Using the same dye concentration, an absorbance spectrum is measured from 650 to 350nm and agrees with the dye absorption spectrum from the manufacturer (Figure B.4).

B.8 Checking the Wavelength Calibration using a Mercury UV Lamp

A mercury UV lamp is used to verify the calibration of wavelength for the spectrophotometer. The procedure on pp. 4-3 of the spectrophotometer's manual[30] is followed. An absorbance spectrum is measured from 450 to 225nm showing absorption peaks that are consistent with the manufacturer's calibration data[30] (Figure B.5).

B.9 Figures
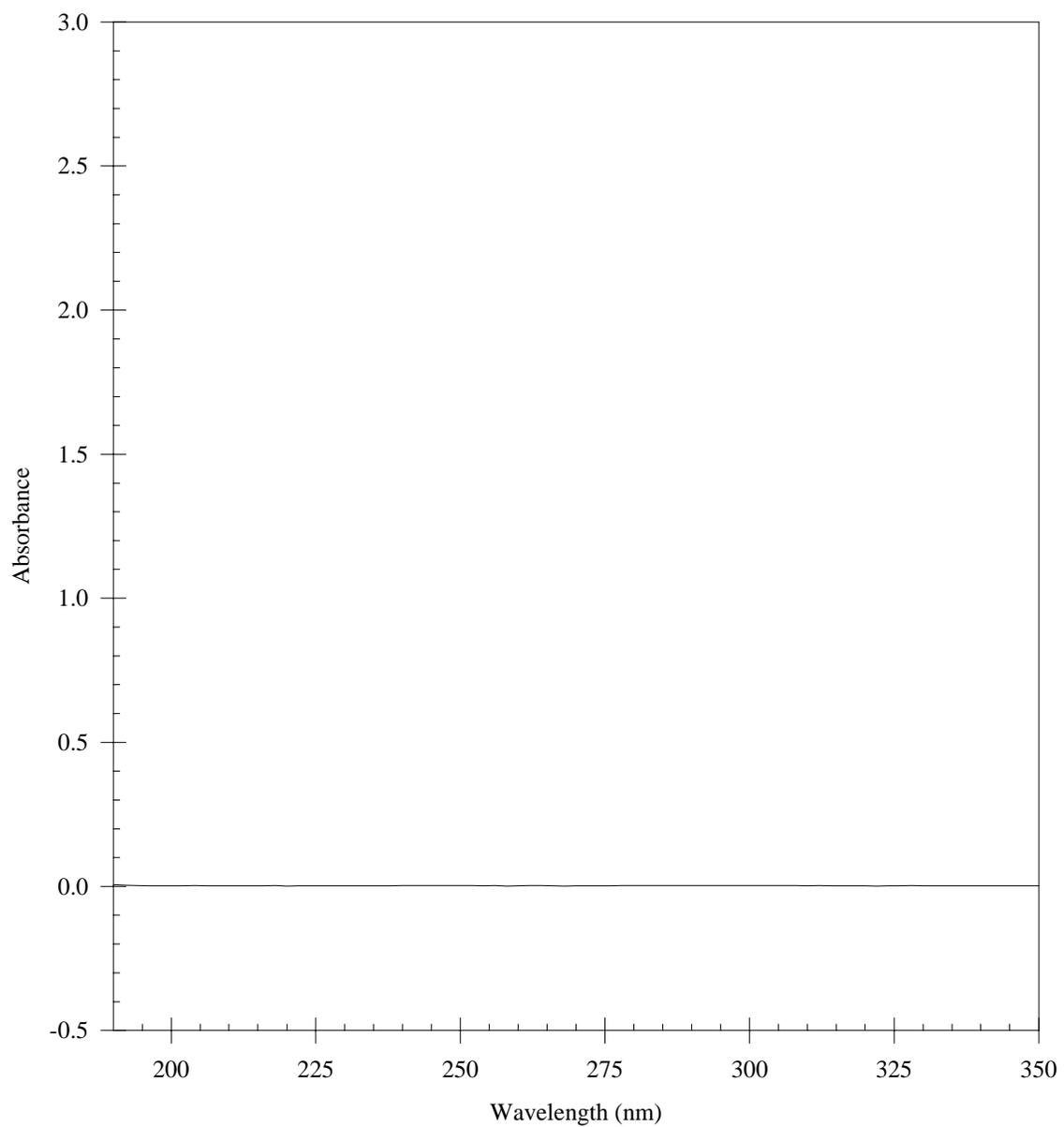
Figure B. 1: The zero absorbance baseline for the UV wavelengths using a dual-beam

UV-VIS-IR spectrophotometer (Varian Associates) with the two apertures of

4mm in diameter present in both the reference and sample chambers to

collimate the incident and transmitted beams.
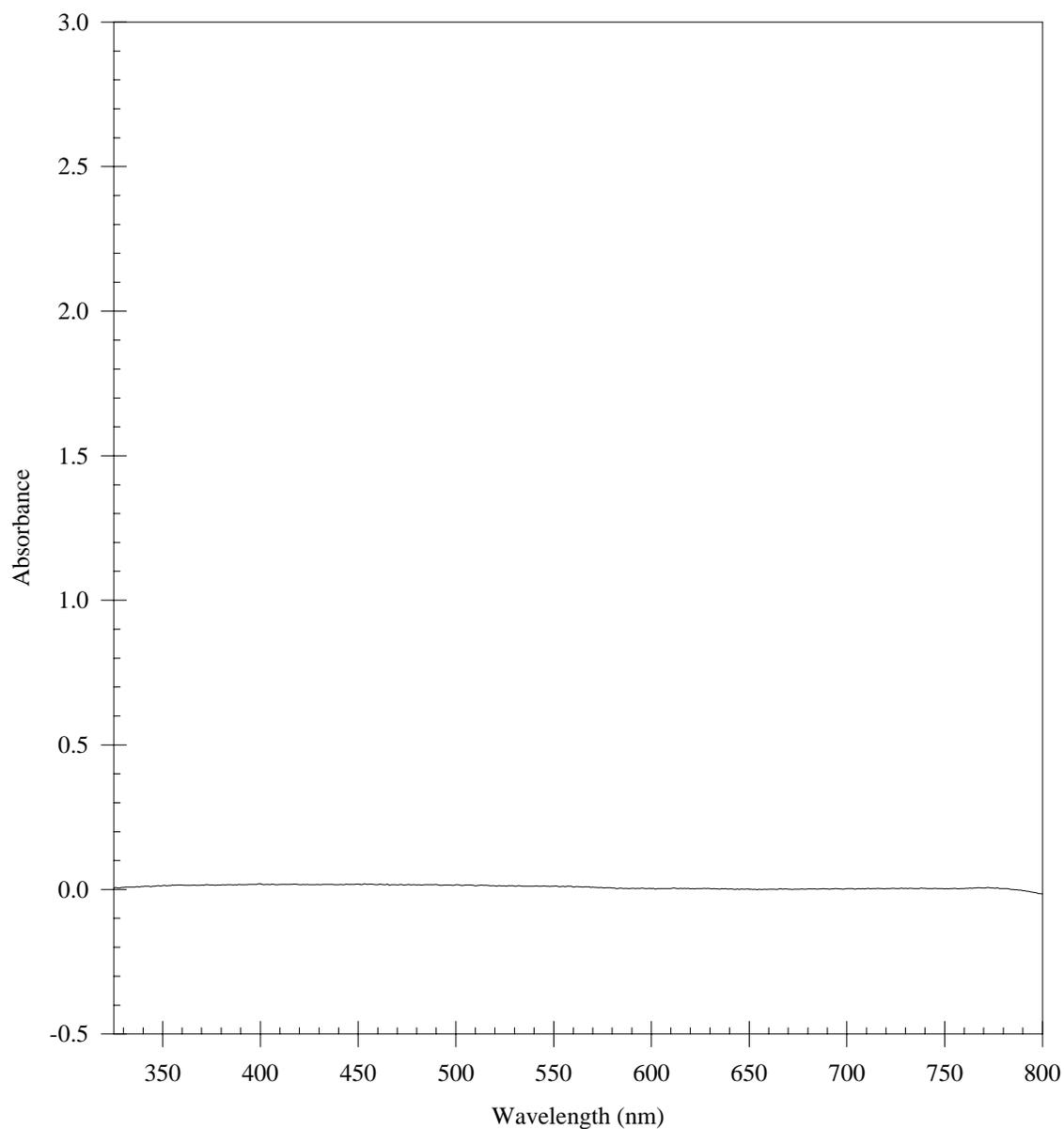
Figure B. 2: The zero absorbance baseline for the VIS wavelengths using a dual-beam

UV-VIS-IR spectrophotometer (Varian Associates) with the two apertures of

4mm in diameter present in both the reference and sample chambers to

collimate the incident and transmitted beams.
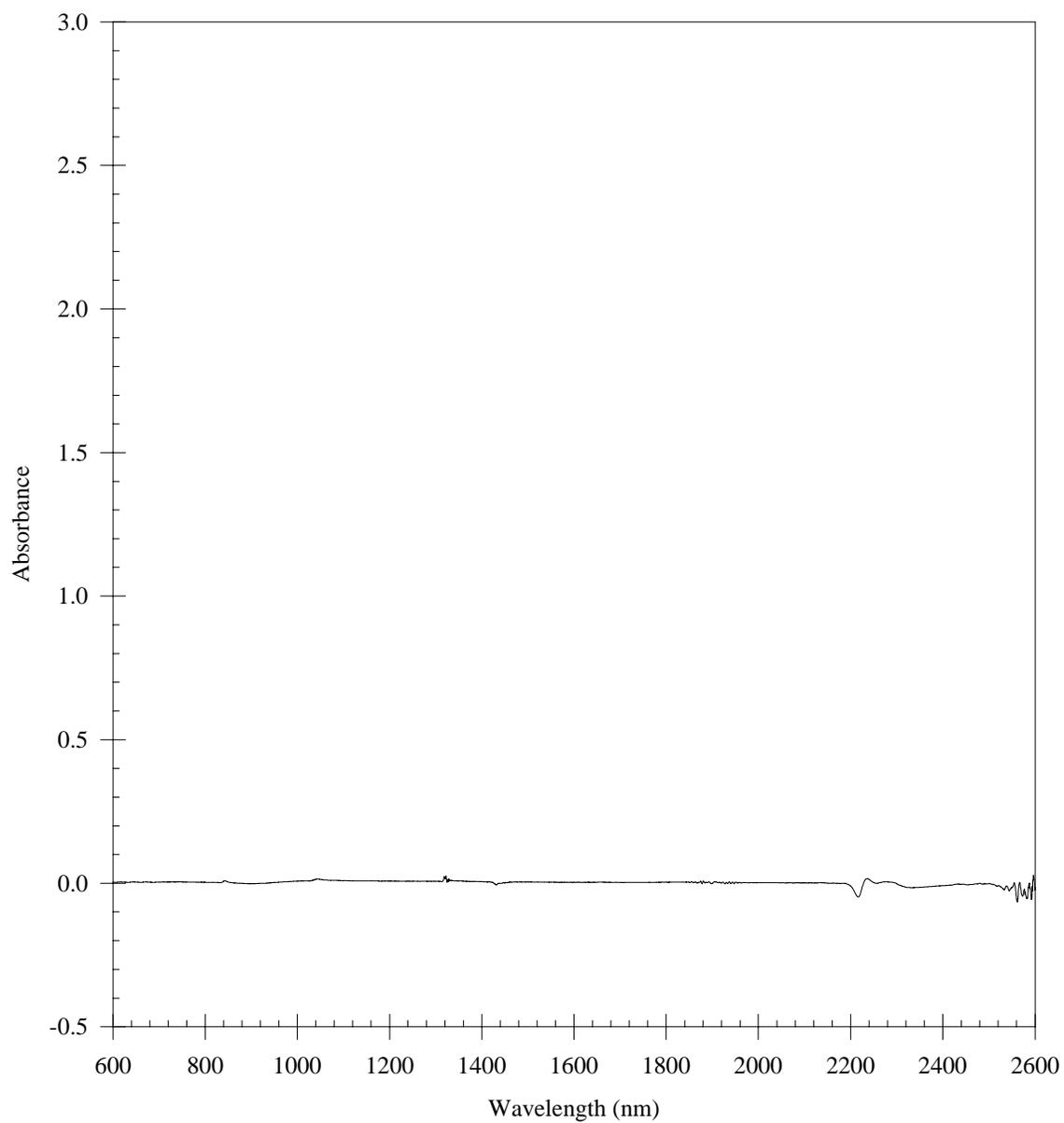
Figure B. 3: The zero absorbance baseline for the VIS-IR wavelengths using a dual-beam

UV-VIS-IR spectrophotometer (Varian Associates) with the two apertures of

4mm in diameter present in both the reference and sample chambers to

collimate the incident and transmitted beams.
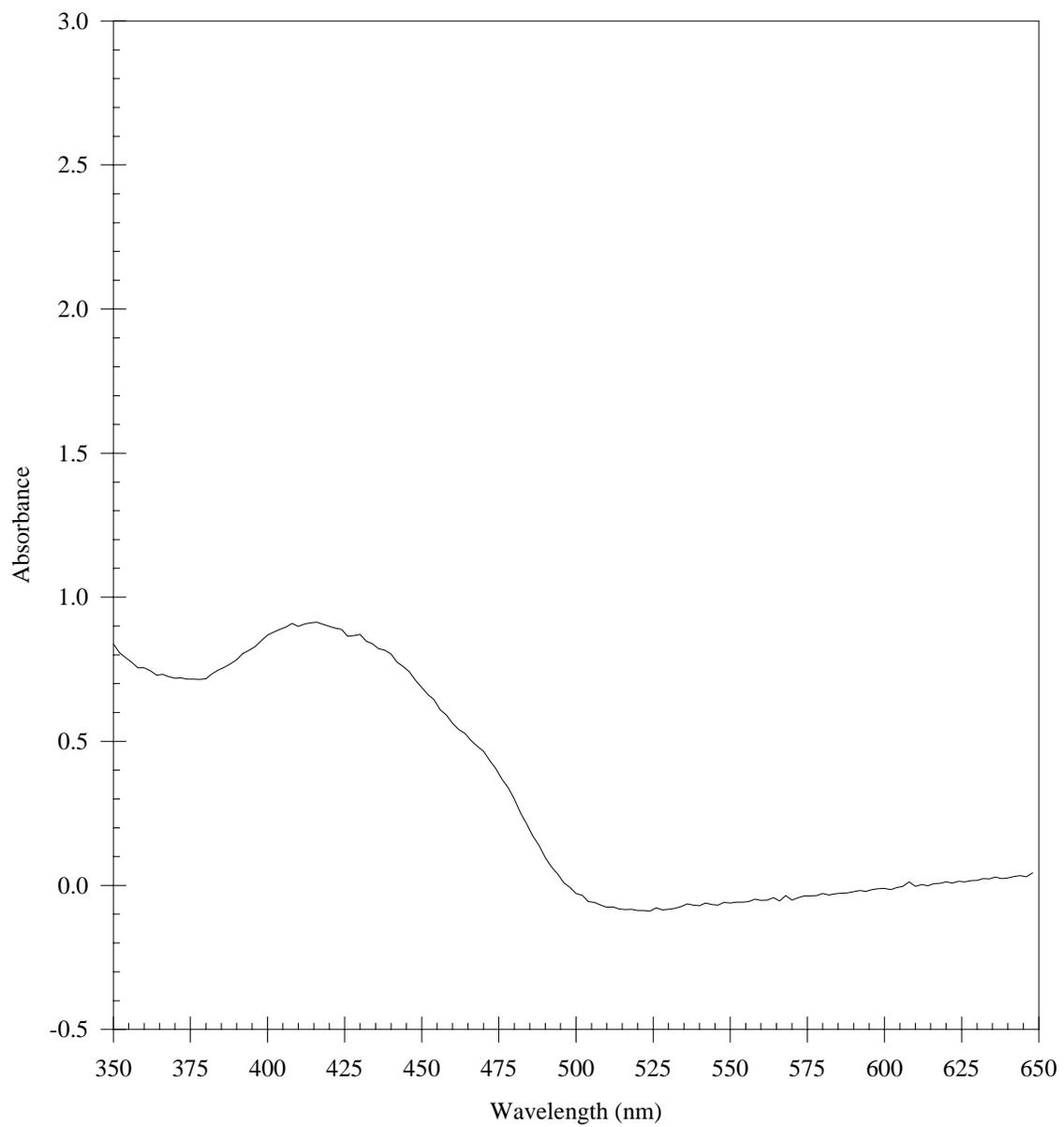
Figure B. 4: The absorbance spectrum of a standard dye solution (Epolite 111-125) of a

concentration of 3mg/l which has a maximum wavelength of 949nm.

63
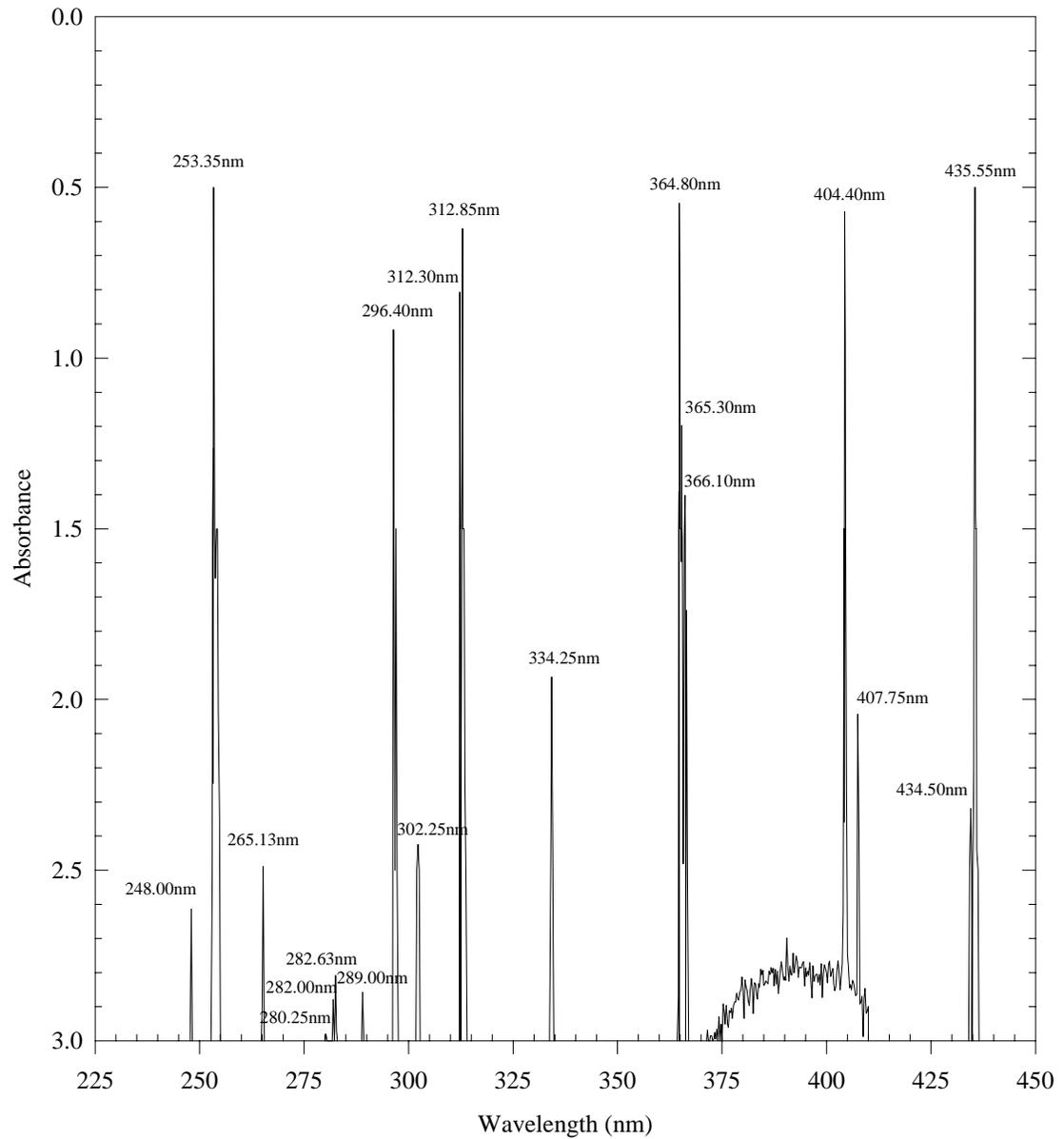
Figure B. 5: The absorbance spectrum of a mercury UV lamp from 450nm to 225nm

used test the wavelength calibration of the spectrophotometer.

Appendix C: Procedure for UV Absorbance Spectra of Corneas

C.1 Set-up Parameters

C.1.1 Spectrophotometer Settings

Slit Knob: 3.0

Pen Period: 1.0

Lamp Source: UV High

Multipots: UV

Scan Speed: 0.05nm/sec

Detector: UV/VIS

Wavelength Counter: set on 350nm or 260nm

Absorbance Suppression: 0.0 but changes throughout spectrum

C.1.2 Data Acquisition Parameters for Computer Program

Number of points was usually set at 2000

Time between each data point: 5 seconds

C.2 Procedure for Measuring Absorbance

1. The spectrophotometer is allowed to warm up for 1 hour while the parameters are set

   on the settings to be used during the scan to allow the electronics to come to an

   operating temperature.

2. Once the spectrophotometer is warmed up, a cornea section is obtained and placed in the sample holder in the sample compartment. Both the reference compartment and the sample compartment are closed.

3. The absorbance reading is taken at 350 or 260nm with the Absorbance Suppression set at 0.0. If the reading is exceeds the scale, the Absorbance Suppression setting is increased until the absorbance reading is on scale. The Absorbance Suppression setting is noted and the scan is taken.

4. When the absorbance reading during the scan exceeds the scale, the scan was stopped, data saved, and wavelength noted. The Absorbance Suppression setting is increased or decreased by one scale and the scan is resumed while overlapping the previous scan by ~5nm. The wavelength at which the scan begins and the new Absorbance Suppression setting are noted.

5. The previous step is repeated until a full spectrum is obtained to 190nm.

6. Once the spectrum is completed, the sample holder is removed from the sample compartment and the cornea thickness is obtained.

7. The cornea thickness is obtained by taking the difference of the sample holder with and without the cornea section.

8. The data is then plotted on SigmaPlot.

9. To convert the computer data into total absorbance (which includes the absorbance of the cornea section and sample holder), the computer data is imported and the

following formula is used:

Total Absorbance Measurement =

$$(\frac{computer\ data}{4096}) + Absorbance\ Suppression \qquad \text{(C.1)}$$

10. The portions of the spectrum that overlapped are averaged.

11. The total absorbance measurement, including the absorbance of the cornea section and the sample holder, is subtracted by the absorbance of the sample holder to obtain the absorbance of the cornea section.

12. The absorbance measurement of the cornea section is then plotted as a function of wavelength.

Appendix D: Procedure for VIS-IR Absorbance Spectra of Corneas

D.1 Set-up Parameters

D.1.1 Spectrophotometer Settings

Slit Knob: 3.0

Pen Period: 1.0

Lamp Source: VIS-IR adjustable

Lamp Voltage: 90V

Multipots: IR

Scan Speed: 0.5nm/sec

Detector: IR

Wavelength Counter: set on 2600nm

Absorbance Suppression: 0.0 but changes throughout spectrum

D.1.2 Data Acquisition Parameters for Computer Program

Number of points was usually set at 205

Time between each data point: 2 seconds

D.2 Procedure for Measuring Absorbance

1. The spectrophotometer is allowed to warm up for 1 hour while the parameters are set

on the settings that are going to be used during the scan to allow the electronics to

come to an operating temperature.

2. Once the spectrophotometer is warmed up, a whole excised cornea is obtained and placed in the sample holder in the sample compartment. Both the reference compartment and the sample compartment are closed.

3. The absorbance reading is taken at 2600nm with the Absorbance Suppression set at 0.0. If the reading exceeds the scale, the Absorbance Suppression setting is increased until the absorbance reading is on scale. The Absorbance Suppression setting is noted and the scan is taken.

4. When the absorbance reading during the scan exceeds the scale, the scan is stopped, data saved, and wavelength and the number of computer data points noted. Then the Absorbance Suppression setting is increased or decreased by one scale and the scan is resumed while overlapping the previous scan by ~5nm. The wavelength at which the scan begins and the new Absorbance Suppression setting are noted.

5. There is a 5% error in the computer's timer that is more critical in scans over 200nm. Therefore, the scan is stopped and resumed, while overlapping the previous scan by ~5nm, every 200nm if the absorbance reading during the scan does not exceed the scale of the spectrophotometer first.

6. The previous steps are repeated until a full spectrum is obtained to 600nm.

7. Once the spectrum is completed, the sample holder is removed from the sample compartment and the cornea thickness is obtained.

8. The cornea thickness is obtained by taking the difference of the sample holder with and without the cornea.

9. The data is then plotted on SigmaPlot.

10. To convert the computer data into absorbance, the computer data is imported and the following formula is used:

Total Absorbance Measurement =

$$(\frac{computer\ data}{4096}) + Absorbance\ Suppression \qquad \text{(D.1)}$$

11. The portions of the spectrum that overlapped are averaged.

12. The total absorbance measurement, including the absorbance of the cornea and the sample holder, is subtracted by the absorbance of the sample holder to obtain the absorbance of the cornea.

13. The absorbance measurement of the cornea is then plotted as a function of wavelength.

Appendix E: Preparing Porcine Skin Tissue Slides

The histology technique chosen to quantitatively measure the ablation depth as a function of laser pulse energy and spot size insures the minimum amount of artifacts and ablation cut distortion. It is important to use a fixer that will penetrate quickly without causing the tissue to become to brittle to section. The amount of time for the dehydration, clearing, and infiltration processes is a difficult obstacle due to the thickness of the skin samples and the fat concentration. The timing sequences for the dehydration, clearing, and infiltration with paraffin in the tissue are based on the visually averaged thickness of the tissue. For skin samples that are thicker than the average, another 30 minutes is added to each step of the of the dehydration, clearing and infiltration procedures. However, a shorter time is never used than stated in the following procedure. The remainder of the technique mirrors that presented in many histology references.[25,31,32]

E.1 Fixation

After ablation, the skin is trimmed and placed in 10% Buffered Formalin for at least 24 hours.

E.2 Dehydration

1. After 24 hours, the formalin in the vial containing the skin is removed with a pipette and replaced with 70% ETOH for at least 30 minutes. The skin may remain in the 70% ETOH until ready to proceed.

2. After at least 30 minutes, the 70% ETOH in the vial containing the skin is removed with a pipette and replaced with 95% ETOH. Once this is done, the procedure must be followed through to step 3 of Clearing. The skin should remain in the 95% ETOH for 30 minutes.

3. After 30 minutes, the 95% ETOH in the vial containing the skin is removed with a pipette and replaced with Absolute Alcohol. The skin should remain in the Absolute Alcohol for 30 minutes.

E.3 Clearing

1. After 30 minutes, the Absolute Alcohol in the vial containing the skin is removed with a pipette and replaced with Xylene. If the Xylene turns cloudy immediately after its addition, then the skin is returned to Absolute Alcohol for another 30 minutes to remove the remaining water in the skin. The skin should remain in the Xylene for 30 minutes.

2. After 30 minutes, the Xylene in the vial containing the skin is removed with a pipette and replaced with 1:1 Xylene:Methanol Salicylate. The skin should remain in the 1:1 Xylene:Methanol Salicylate for 30 minutes.

3. After 30 minutes, the 1:1 Xylene:Methanol Salicylate in the vial containing the skin is removed with a pipette and replaced with Methanol Salicylate. The skin should remain in the Methanol Salicylate for at least 30 minutes. The skin may remain in the Methanol Salicylate until ready to proceed.

E.4 Infiltration

1. After at least 30 minutes, the Methanol Salicylate in the vial containing the skin is removed with a pipette. The skin is then transfer to melted Paraplast in a dish and placed in an oven (set at 60°C, which is 2 or 3° above the melting point of Paraplast) for 1 hour.

2. After 1 hour, the paraffin is poured off the skin into a waste container and the dish is refilled with fresh Paraplast. The dish is then returned to the oven for another hour.

3. After another hour, the paraffin is poured off the skin into a waste container and the dish is refilled with fresh Paraplast. The dish is then returned to the oven for another hour.

E.5 Embedding

1. During the last hour of infiltration, a metal mold should be prepared for the embedding process. The metal mold is coated with glycerine to prevent the Paraplast from adhering to it.

2. The dish containing the skin sample is removed from the oven and the excess paraffin is poured into the waste container. The dish is then placed on a hot plate.

3. Melted Paraplast is then poured into the mold. The bottom and the sides are allowed to solidify. The top portion of the paraffin is stirred with a warm needle to prevent it from hardening in the center.

4. The skin sample is placed in the metal mold filled with paraffin and a warm needle is used to orientate the skin sample in the position necessary for slicing. In this case, the

skin sample is place flat so the ablation cuts are perpendicular to the face of the block
that will be cut.

TOP VIEW

Face of block
to be cut.
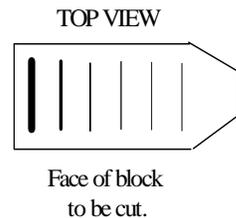
5. The skin sample in the metal mold filled with paraffin is allowed to solidify at room
   temperature. Once solidified the sample block is removed from the metal mold.

6. If crystallization occurs during the solidification process, then the skin sample is
   returned to fresh Paraplast in a dish to allow the paraffin to liquefy and the embedding
   procedure is repeated.

7. The embedded sample may be stored indefinitely in a cool place.

E.6 Preparing the Sample Block and Microtome for Sectioning

1. The sample block is trimmed so the skin sample is barely visible in the paraffin.
   Trimming of the block is done to have a small surface area to section, with the full
   sample intact.

2. The microtome is cleaned of debris and reset to its initial positions.

3. The hand wheel is locked and left so the sample block holder is in its highest position.

4. The sample block is clamped into the chuck of the sample block holder.

5. The face of the paraffin block is adjusted horizontally and vertically so that the
   sample block's upper and lower edges are parallel with the base of the microtome.

6. The blade edge is cleaned with Xylene and placed in the microtome holder. The angle of the blade should be approximately 20°.

7. The hand wheel is unlocked and the sample block is positioned so it is level with the knife blade.

8. The knife holder is unlocked and positioned so the knife's edge is almost in contact with the face of the sample block. The knife holder is then locked back into position.

9. The desire thickness of the sections is set at 10μm.

E.7 Sectioning of the Sample Block

1. The hand wheel is turned at a steady rhythm.

2. Several sections are cut until the center of the ablation cuts is reached (approximately 1 to 1.5cm into the skin sample).

3. Once the center of the ablation cuts is reached and the previous sections are discarded, a ribbon of sections about 10cm long is cut.

4. The ribbon is detached from the knife's edge and laid on a flat surface.

5. When finished obtaining all of the necessary ribbons, the knife blade is cleaned with Xylene and placed in the refrigerator.

E.8 Preparing the Slides

1. The slides are first cleaned with acid and 70% ETOH and then labeled.

2. The ribbons are divided into sections containing 5 to 7 sample sections.

3. A drop of albumen is placed on a cleaned slide and rubbed into the surface of the slide with a clean finger. The excess albumen is removed with tissue paper.

4. The albumenized surface is covered with a thin layer of distilled water.

5. Using forceps, a ribbon section containing 5 to 7 sample sections is placed on the thin layer of distilled water.

6. The slides are placed on a covered warming table (set at 42°C), in order to remove wrinkles in the sections, overnight.

E.9 Staining the Slides

1. The slides are removed from the warming table and allowed to cool to room temperature.

2. For each of the following steps, the slides are drained on a paper towel between the solutions and left in the solutions for the appropriate time limit.

3. Xylene (3 minutes)

4. Xylene (3 minutes)

5. 100% ETOH (2 minutes)

6. 95% ETOH (2 minutes)

7. 70% ETOH (2 minutes)

8. A jar was placed in the sink and cold tap water is allowed to drip rapidly on the slides (3 minutes)

9. Delafield's (or Harris) Hematoxylin (5 Minutes)

10. Running tap water as in Step 3 (3 minutes)

11. 70% ETOH (3 minutes)

12. 70% ETOH (2 minutes)

13. Eosin (1 minute)

14. 95% ETOH (a few seconds)

15. 100% ETOH (2 minutes)

16. 100% ETOH (2 minutes)

17. Xylene (3 to 15 minutes)

18. Removing one slide from the Xylene at a time, a drop of thin mounting medium is placed over the wet sections and carefully covered with a clean cover slip (avoiding air bubbles).

19. The slides are store in the horizontal position until dry.

Appendix F: Student's *t*-test

When looking at confidence intervals for small sample sizes, the normal distribution may give substantial errors in determining the correlation between sample populations. An exact confidence interval can be obtained through the use of the Student's *t* distribution. The *t* distribution is a probability distribution similar to the normal distribution but with important differences. It is defined as a probability distribution often used when the population standard deviation is not known or when the sample size is small.[33] For determining the correlation between the average linear absorption coefficients for the porcine and human corneas, the Student's *t* test is chosen because the sample size is less than 30.

For the purposes of this study, the unpaired Student's *t* test is used to test the correlation between two independent sample averages $\overline{\alpha}_i$. It is assumed, however, that the two sample populations are each normally distributed with the same standard deviation σ_i. In looking at the linear absorption coefficients $\overline{\alpha}_i$ for both the porcine and human corneas, the standard deviations σ_i are within 60cm^{-1}. We want to test the correlation between the difference of the calculated $\overline{\alpha}_i$ and the hypothesized difference of the population means μ_i. The relevant *t* ratio for testing the difference between two independent averages following the above assumption is given by[33,34]:

$$t = \frac{(\overline{\alpha}_1 - \overline{\alpha}_2) - (\mu_1 - \mu_2)}{\sqrt{\frac{(n_1 - 1)\sigma_1^2 + (n_2 - 1)\sigma_2^2}{n_1 + n_2 - 2}\left(\frac{1}{n_1} + \frac{1}{n_2}\right)}} \qquad (F.1)$$

which is the unpaired Student's *t*-test with degrees of freedom ($n_1 + n_2 - 2$) where $\bar{\alpha}_i$ is

the average linear absorption coefficient for our sample of the population i, n_i is the

sample size, σ_i is the standard deviation of $\bar{\alpha}_i$, and μ_i is the average linear absorption

coefficient for the population i.

To determine the correlation between the porcine and human cornea's linear

absorption coefficients $\bar{\alpha}$ at 220, 215, 210 and 193nm, the *t* ratio is found using Eq. (F.1)

where the difference in the population averages is assumed to be zero, which is referred

to as the null hypothesis. By evaluating against the null hypothesis, we are determining

the probability that the sample means are the same.

Once the *t* ratio is calculated, a confidence level is chosen to evaluate if the null

hypothesis should be rejected.[33,34] For the cornea data, a 95% confidence level is chosen

using the two-tail approach. The two-tail approach tests if the probability is divided

between both the tails of distribution. Therefore, the probability of a difference in $\bar{\alpha}$ is

not dependent on the direction of distribution. Once the *t* ratio is calculated, it is

compared to the table of critical *t* ratios for a specific confidence level and a

corresponding degree of freedom. It is found that the calculated *t* ratio is less than the

critical value of *t* at the 95% confidence level for the four wavelengths. This indicates

that the null hypothesis is valid and shows that the average linear absorption coefficients

have a 95% probability of being equivalent. Therefore, it is determined that the linear

absorption coefficients of the porcine and human corneas are less than 5% significantly

different. Because $\overline{\alpha_i}$ is determined from a random sampling of the population, we also

conclude that μ_i is the same value as $\overline{\alpha_i}$.